Long-term (1990-2019) monitoring of tropical moist forests dynamics

C. Vancutsem[1]*, F. Achard[1], J.-F. Pekel[1], G. Vieilledent[1,2], S. Carboni[3], D. Simonetti[1], J. Gallego[1], L. Aragao[4], R. Nasi[5]

[1] European Commission, Joint Research Centre, Via E. Fermi 2749 – TP 261, I-21027 Ispra (VA), Italy.

[2] CIRAD, UPR Forêts et Sociétés, F-34398 Montpellier, France.

[3] GFT Italia Srl, Milan, Via Sile 18, Italy.

[4] National Institute for Space Research (INPE), São José dos Campos, Brazil.

[5] Center for International Forestry Research (CIFOR), Bogor, Indonesia.

*Correspondence to: Christelle.vancutsem@gmail.com

ABSTRACT

Accurate characterization of the tropical moist forests changes is needed to support conservation policies and to better quantify their contribution to global carbon fluxes. We document - at pantropical scale - the extent of these forests and their changes (degradation, deforestation and recovery) over the last three decades. We estimate that 17% of the tropical moist forests have disappeared since 1990 with a remaining area of 1060 million ha in 2019, from which 8.5% are degraded. Our study underlines the importance of the degradation process in such ecosystems, in particular as precursor of deforestation and in the recent increase of the tropical moist forest disturbances. Without reduction of the present disturbance rates, undisturbed forests will disappear entirely in large tropical humid regions by 2050. Our study suggests reinforcing actions to prevent the first disturbance scar that leads to forest clearance in 45% of the cases.

INTRODUCTION

Tropical moist forests (TMF) have a huge environmental value. They play an important role in biodiversity conservation, terrestrial carbon cycle, hydrological regimes, indigenous population subsistence and human health (**1-5**). They are increasingly recognized as an essential element of any strategy to mitigate climate change (**6, 7**). Deforestation, and degradation compromise the functioning of tropical forests as an ecosystem, lead to biodiversity loss (**1, 4, 5, 8, 9)** and reduced carbon storage capacity (**10-17**). Deforestation and fragmentation are increasing the risk of virus disease outbreaks (**18-20**).

For humanity wellbeing, sustainable economic growth and conservation of the remaining TMF constitute one of the largest challenges and shared responsibility. A consistent, accurate and geographically explicit characterization of the long-term disturbances at the pantropical scale is a prerequisite for elaborating a coherent territorial planning towards Sustainable Development Goals (SDGs) and the Nationally determined contributions (NDCs) of the Paris Agreement (2015). Advances in remote-sensing, cloud computing facilities, and free access to the Landsat satellite archive (**21-23**)**,** enable systematic monitoring and consistent dynamic characterization of the entire TMF across a long period. Global maps have been derived to quantify tree cover loss since 2000 (**24-25**) and to identify remaining intact forest landscapes (**17**). However, detailed spatial information on the long-term dynamics of tropical moist forests and particularly on forest degradation and post-disturbances development stages is still missing to accurately estimate the carbon loss associated with forest disturbances (**2, 13, 15**) and assess their impact on biodiversity (**5, 8**).

RESULTS AND DISCUSSION

Here we provide new information through a wall-to-wall mapping of tropical moist forest cover dynamics over a long-term period (January 1990 to December 2019) at 0.09 ha resolution (freely available from https://forobs.jrc.ec.europa.eu/TMF/) (see Materials and Methods). This validated dataset depicts the TMF extent and the related disturbances (deforestation and degradation), and post-disturbances recovery on an annual basis over the last three decades (see Supplementary Text on the annual change dataset, and fig. S1). A major innovation consists of characterizing the sequential dynamics of changes by providing transition stages from the initial observation period to the end of the year 2019, i.e. undisturbed forest, degraded forest, forest regrowth, deforested land, conversion to plantations, conversion to water, afforestation, and changes within the mangroves (**Figs. 1 and 2**, see Supplementary Text on the transition map and figs. S2 to S7), as well as the timing (dates and duration), recurrence and intensity of each disturbance.

For the first time at the pantropical scale the occurrence and extent of the forest cover degradation is documented on an annual basis in addition to the deforestation. This has been achieved thanks to the analysis of each individual valid observation of the Landsat archive (see Data and Mapping method Sections) allowing to capture short-duration disturbances such as selective logging (**Fig. 2F**, fig. S3), fires (**Fig. 2B)**, and severe weather events (hurricanes, dryness) (fig. S7).

The accuracy of the disturbance mapping is 91.4%. Uncertainties in the area estimates were quantified based on a sample-based reference in accordance with the latest statistical good practices (**26**) and indicates an underestimation of the forest disturbance areas by 11.8% (representing 38.4 million ha, with 15 million ha confidence interval at 95%) (see Section and Supplementary Text on the validation, figs. S8 to S10 and tables S1 to S4).

72 ***Main results on degradation***

73 The analysis of the yearly dynamics of TMF disturbances over the last 30 years underlines the
74 importance of the degradation process in tropical moist forest ecosystems with the following key
75 outcomes (**Tables 1, 2 and 3**, the Trend analysis section in Materials and Methods, fig. S11):

76 (i) During the last three decades, 195.1 million ha of TMF have disappeared and
77 106.5 million ha are in a degraded status (**Table 3**). This represents 8.4% of the 1059.6
78 million ha of forest area remaining in January 2020. Degraded forests represent 33% of
79 the observed disturbances with high variability between regions and countries, ranging
80 from 96% in Venezuela, 74% in Gabon, and 69% in Papua New Guinea to 21% in Brazil
81 and Madagascar, and 13% in Cambodia (Table S6). 40.7% of the degraded forests are
82 in Asia-Oceania (compared to 36.9% in Latin America and 22.3% in Africa) (**Table 3**).
83 (ii) 84.5% of the degraded forests (i.e. 90 million ha) are resulting from short-term
84 disturbances (observed over less than 1-year duration, mostly due to selective logging,
85 natural events and light-impact fires), from which 30 million ha have been degraded
86 repeatedly 2 or 3 times over the last 30 years (observed each time along a short-term
87 period). The remaining 15.5% (16.5 million ha) are mainly resulting from intense fires,
88 with a disturbance duration between 1 to 2.5 years.
89 (iii) 45.4% of the degradation (88.6 million ha) is a precursor of deforestation events
90 occurring on average after 7.5 years (without significant variability between continents).
91 This is particularly true for South-East Africa and South-East Asia that show
92 respectively 60.4% (with 65% for Madagascar) and 53% (with 59% for Cambodia) of
93 degraded forests becoming deforested in a second step (**Table 2**). These proportions are
94 underestimated because 45.4% of recent degradation (e.g. in the last 7 years) will most
95 likely be deforested in future years.

(iv) A further 30.3% of the undisturbed forest areas (291.8 million ha) are potentially disturbance-edge-affected forests, i.e. located within 120 meters from a disturbance (see Materials and Methods). This proportion indicates a higher forest fragmentation proportion in Asia (45.2%) compared to other continents (25.6% and 28.9% respectively in the Americas and Africa).

(v) 82.8% of the TMF mapped as degraded in December 2019 corresponds to short-term disturbances that have never been identified so far at the pan-tropical scale. Over the period covered by the Global Forest Change (GFC) product (**24**), i.e. 2001-2019, 21.2 million ha have been captured as a tree cover loss compared to 86 million ha detected as degraded forests by our study during the same period (see Section on the comparison with the GFC dataset, **Fig. 4** and table S5).

(vi) We show that the annual rate of degradation is highly related to climatic conditions (**Figs. 3 and 4**, fig. S11). Whereas the trends in deforestation rates seem to be related to changes in national territorial policies, degradation rates usually show peaks during drought periods and do not seem to be impacted by forest conservation policies. The drought conditions that occurred during strong and very strong El Niño southern oscillation (ENSO) events of 1997-1998 and 2015-2016 were optimal for forest fires (**27-29**) and resulted in a strong increase of forest degradation (**28**). The impact of these fires in 2015-2016 is particularly strong and visible in all regions except in South-East Africa.

Our results stress the paramount importance of (i) integrating measures for reducing degradation in forest conservation and climate mitigation programs, and (ii) considering forest degradation as risk factor of deforestation and as an indicator of climate change and climate oscillations. We anticipate that a better knowledge of forest degradation processes and its resulting fragmentation will help to

assess accurately the anthropogenic impact on the tropical ecosystem services and the effects on biosphere-atmosphere-hydrosphere feedbacks. Future policies will have to account for this finding.

Main results on deforestation and post-deforestation regrowths

Deforestation in TMF cover is documented in an unprecedented comprehensive manner: (i) by covering a 30-year period of analysis, (ii) by mapping deforestation occurring after degradation and deforestation followed by a regrowth, (iii) by identifying specific forest conversion to commodities or water (**Figs. 2G and 2I**), (iv) by including changes within the mangroves (**Fig. 2A)**, and (v) by documenting each deforestation event at the pixel level by its timing (date and duration), intensity, recurrence and when appropriate, start date and duration of post-disturbance regrowth.

Overall, 17.2% of the initial TMF area (i.e. 207.4 over 1267.1 million ha), have disappeared since 1990, down to 1059.6 million ha of TMF in January 2020 (**Tables 1, 2 and 3**). We report a rate of gross loss of TMF area for the entire pan-tropical region varying from 5.5 to 7.7 million ha / year with the period (**Table 4**). Comparison with previous studies results in the following outcomes:

(i) Estimations reported by FAO national statistics (**30**) and the sample-based estimations from Tyukavina *et al*. (**31**) for the natural tropical forest – that includes both moist and dry forest types - are higher by 0.9% and 27% respectively, compared to our TMF deforestation rates (excluding the conversion to tree plantations to get closer to the natural forest definition of these two studies) for the same period (**Table 4**). At the continental scale, Tyukavina *et al*. (**31**) shows lower estimates than our study for Africa (-23%) and for Asia (-4%), and higher estimates for Latin America (+16%).

(ii) Comparison with GFC loss (**24**) (see Section on the Comparison with the GFC dataset and **Fig. 4**) shows a lower deforestation rate (-33%) compared to our study for the period 2000-

2012 over the same forest extent (using our TMF extent for the year 2000) (**Table 4**). Underestimation of GFC loss has been documented by previous studies (**31, 33**). Tyukavina *et al*. (**31**) reported an underestimation of GFC loss of 19.4% considering the entire forest cover (moist and deciduous) loss during the period 2001-2012, with a larger underestimation for Africa (-39.4%) compared to other continents (-13% for Latin America and -5.7% for Asia). The ranking of this underestimation by continent is consistent with the ranking observed in our study (first Africa, second Latin America and third Asia). The differences with GFC loss are explained by three specific assets of our approach: (i) the use of single-date images enabling the detection of short-duration disturbance events (i.e. visible only during a few weeks from space) compared to the use of annual syntheses, (ii) a dedicated algorithm for TMF enabling the monitoring of seven forest cover change classes compared to the global monitoring of forest clearance, and (iii) a cloud masking and quality control optimized for equatorial regions enabling a more comprehensive analysis of the Landsat archive.

(iii) Comparison with the Brazilian PRODES data (**29**) using their primary forest extent (**Fig. 4**) shows a similar decrease of annual deforestation rates between the 2000's and the last decade that can be related to a set of economic and public policy actions (**28**). Differences in the deforestation rates are observed (i) during the period 2001-2004 with a higher deforestation rate for PRODES (2.32 million ha/year) compared to our study (2 million ha/year) and to GFC loss (1.53 million ha/year), and (ii) in the last ten years with a lower average deforestation rate for PRODES compared to our study and GFC loss (0.67, 1.1 and 1.34 million ha/year respectively) (**Table 4**). These differences are accentuated in the last five years (0.77, 1.33, and 1.76 million ha/year respectively). Discrepancies in area estimates between our product and the PRODES data are explained by (i) difference in minimum mapping units (0.09 ha compared to 6.25 ha in PRODES), and (ii) impacts of

strong fires that are captured in our study (deforestation followed by forest regrowth) and in GFC loss but are discarded in the PRODES approach (because not considered as deforestation).

This study documents – in an unprecedented manner - the extent and age of post-deforestation regrowths (young secondary forests that are regenerating after human or natural disturbance) for the entire pan-tropical domain. These secondary forests grow rapidly in tropical moist conditions and absorb large amounts of carbon, whereas they were poorly documented. We show that 13.5% of the deforested areas (i.e. 29.5 Million ha) are regrowthing in a subsequent stage, with 33% of these secondary forests aged more than 10 years at the end of 2019 (**Table 3**). The proportion of secondary forests within the total deforestation is higher in Asia (18.3%) compared to Latin America (12.3%) and Africa (7.9%). The disturbance events followed by a forest regrowth are including intense fires and these are accentuated by drought conditions. This is well visible for South America (**Fig. 3**) for years 1997-1998 and 2010. Additionally, 10 Million ha are characterized as evergreen vegetation regrowth of areas initially classified as non-forest cover, i.e. that can be considered as forestation (i.e. afforestation and reforestation) aged of more than 10 years.

This study confirms that most of the deforestation caused by the expansion of oil palm and rubber and assigned to the commodity classes in our study (see Supplementary Text on ancillary datasets, **Figs. 2I and 3B**, Fig. S11 and table S6) is concentrated in Asia with 18.3 million ha (representing 86% of the entire TMF conversion to plantations), and more specifically in Indonesia (57.4%) and Malaysia (23.8%).

194 ***Deforestation and degradation trends***

195 The evolution of the deforestation and degradation over the last three decades show the highest
196 peaks of annual disturbances in Latin America and Southeast Asia during the period 1995-2000
197 with 6.3 million ha/year and 6.2 million ha/year respectively. The ENSO of 1997-1998 may - at
198 least partially - explain these peaks of forest disturbances, in particular for Indonesia and Brazil
199 where such peaks are manifest in the annual change trends with the highest proportion of
200 degradation events over the total disturbance areas (**Figs. 3 and 5**, fig. S11). Between 2000-2004
201 and 2015-2019, the disturbance rates decreased by half in South-America and by 45% in South-
202 East Africa and continental South-Est Asia. Brazil - that accounts for 29% of the remaining world's
203 TMF - largely contributed to this reduction (from 4.3 million ha/year down to 2.1 million ha/year)
204 (**Figs. 3, 4**, **and 5**, **Table 4**, table S6 and fig. S11).
205
206 In the recent years, our study shows a dramatic increase of disturbances rates (deforestation and
207 degradation) (+ 2.1 million ha/year for the last 5 years compared to the period 2005-2014) to reach
208 a level close to that of the early 2000s (**Tables 2 and 3**) with the highest increases observed in West
209 Africa and Latin America (48% higher). Degradation is the main contributor of this recent increase
210 (average increase of 38% whereas annual deforestation decreased by 5%) caused notably by
211 specific climatic conditions in 2015-2016 (**29**) (**Figs. 3 and 5**). Asia-Oceania region shows a lower
212 increase of degradation rate (31%) compared to Africa (34%) and Latin America (49%) and a much
213 higher decrease of deforestation rate (28%) compared to Africa (5%) and Latin America (12%).
214
215
216
217

Undisturbed TMF decline and projections

Since 1990, the extent of undisturbed TMF has declined by 23.9% with an average rate of loss of 10.8 million ha/year. The decline of undisturbed TMF is particularly dramatic for Ivory Coast (81.5% of their extent in 1990), Mexico (73.7%), Ghana (70.8%), Madagascar (69%), Vietnam (67.8%), Angola (67.1%), Nicaragua (65.8%), Lao People's Democratic Republic (PDR) (65.1%), and India (63.9%) (table S6). If the average rates of the period 2010-2019 would remain constant over a short or medium term future (see Materials and Methods, fig. S12), undisturbed TMF would disappear by 2026-2029 in Ivory Coast and Ghana, by 2040 in Central America and Cambodia, by 2050 in Nigeria, Lao PDR, Madagascar and Angola, and by 2065 for all the countries of continental Southeast Asia and Malaysia. By 2050, 15 countries –including Malaysia (the 9th country with the biggest TMF forest) - will lose more than 50% of their undisturbed forests (table S6).

CONCLUSION

It is now possible to monitor deforestation and degradation in tropical moist forests consistently over a long historical period and at fine spatial resolution. The mapping of forest transition stages will allow to derive more targeted indicators to measure the achievements in forest, biodiversity, health and climate policy goals from local to international levels (**34**). Our study shows that tropical moist forests are disappearing at much faster rates than what was previously estimated and underlines the precursor role of forest degradation in this process. These results should alert decision makers on the pressing need to reinforce actions for preserving tropical forest, in particular by avoiding the first scar of degradation that is most likely leading to forest clearance later on.

242 ## MATERIALS AND METHODS

243 ### *Study area and Forest types*

244 Our study covers the tropical moist forests, which include the following *formations* (**35**): the
245 lowland evergreen rain forest, the montane rain forest, the mangrove forest, the swamp forest, the
246 tropical semi-evergreen rain forest, and the moist deciduous forest. Evergreenness varies from
247 permanently evergreen to evergreen seasonal (mostly evergreen but with individual trees that may
248 lose their leaves), semi-evergreen seasonal (up to about one third of the top canopy can be
249 deciduous, though not necessarily leafless at the same time), and moist deciduous (dominant
250 deciduous species with evergreen secondary canopy layer).

251

252 We do not intent to map specifically intact or primary forest as the Landsat observation period is
253 too short to discriminate never-cut primary forest from second growth naturally recovered forest
254 older than the observation period. However, by documenting all the disturbances observed over the
255 last three decades, the remaining undisturbed TMF in 2019 is getting closer to the primary forest
256 extent. Whereas our entire TMF - that includes undisturbed and degraded forests - in 1990 and 2019
257 are comparable, our undisturbed forest of 1990 and 2019 should be carefully compared.

258

259 Our study area covers the following Global Ecological Zones (**36**): 'Tropical rainforest', 'Tropical
260 moist forest', 'Tropical mountain system' and 'Tropical dry forest' (fig. S13) and stops at the
261 borders of China, Pakistan, Uruguay, and USA. The TMF are located mostly in the tropical moist
262 and humid climatic domains but also include small areas of gallery forests in the tropical dry
263 domain.

264

265

266

267 ***Data***

268 The Landsat archive is the only free and long-term satellite image record suited for analysing
269 vegetation dynamics at fine spatial resolution. We used the entire L1T archive (orthorectified top
270 of atmosphere reflectance) acquired between July 1982 and December 2019 from the following
271 Landsat sensors: Thematic Mapper (TM) onboard Landsat 4 and 5, Enhanced Thematic Mapper-
272 plus (ETM+) onboard Landsat 7 and the Operational Land Imager (OLI) onboard Landsat 8 (**23,**
273 **37-39**). Landsat 4 was launched in July 1982 and collected images from its TM sensor until
274 December 1993. Landsat 5 was launched in March 1984 and collected images until November
275 2011. Landsat 7 was launched in April 1999 and acquired images normally until May 2003 when
276 the scan line corrector (SLC) failed (**40**). All Landsat 7 data acquired after the date of the SLC
277 failure have been used in our analysis. Landsat 8 began operational imaging in April 2013.
278
279 The Landsat archive coverage presents large geographical and temporal unevenness (**37, 41**). The
280 main reason for the limited availability of images for some regions is that Landsat 4 and 5 had no
281 onboard data recorders, and links with data relay satellites failed over time; cover was therefore
282 often limited to the line of sight of receiving stations (**39**). Commercial management of the
283 programme from 1985 to the early 1990s led to data acquisitions being acquired mostly when pre-
284 ordered **(37).** From 1999 onwards, the launch of Landsat 7 and its onboard data recording
285 capabilities, associated with the continuation of the Landsat 5 acquisitions, considerably improved
286 global coverage.
287
288 In the tropical regions, Africa is particularly affected by the limited availability of image
289 acquisitions, especially in the first part of the archive. From a total of around 1 370 860 Landsat
290 scenes that were available for our study area, only 265 098 scenes were located in Africa (in
291 comparison, 573 589 and 532 173 scenes were respectively available in South America and Asia).

The most critical area is located around the Gulf of Guinea, with an overall average number of valid observations (i.e. without clouds, hazes, sensor artefacts and geo-location issues) over the full archive (fig. S14) of fewer than 50 per location (pixel) and with the first valid observations starting mostly at the end of the 1990s (fig. S15). Small parts of Ecuador, Colombia, Salomon Islands and Papua New Guinea present a similar low number of total valid observations, often with an earlier first valid observation around the end of the 1980s. Apart from these regions, the first valid observation occurs mostly within periods 1982-1984, 1984-1986, or 1986-1988 for Latin America, Africa and Southeast Asia, respectively.

The average number of annual valid observations (fig. S16) shows a stepped increase during the 38-year period for the three continents, with two major jumps: in 1999 with the launch of Landsat 7, and in 2013 with the launch of Landsat 8. There is also a clear drop in 2012 for Southeast Asia and Latin America with the decommissioning of Landsat 5 in November 2011, and a small drop in 2003 as a consequence of the Landsat 7 SLC off issue. There are major differences between Africa and the two other continents: Africa has significantly fewer valid observations, in particular during the period 1982-1999, and a much larger increase in number of observations from 2013.
The geographical unevenness of the first year of acquisition constrains the monitoring capability period. Our method accounts for this constraint notably by recording the effective duration of the archive at the pixel level (see next subsection).

Data quality issues affecting the Landsat collection were addressed by excluding pixels where (i) detector artefacts occur (manifested as random speckle or striping), (ii) one or more spectral bands are missing (typically occurring at image edges) or (iii) scene geo-location is inaccurate.

317 ***Mapping method***

318 In order to map the area dynamics (extent and changes) of the TMF over a long period, we
319 developed an expert system that exploits the multispectral and multitemporal attributes of the
320 Landsat archive to identify the main change trajectories over the last 3 decades and uses ancillary
321 information to identify sub-classes of forest conversion (see Supplementary Text on Ancillary
322 data). The inference engine of our system is a procedural sequential decision tree, where the expert
323 knowledge is represented in the form of rules. Techniques for big data exploration and information
324 extraction, namely visual analytics (**42**) and evidential reasoning (**43)**, were used similarly to a
325 recent study dedicated to global surface water mapping (**41**). The advantages of these techniques
326 for remotely sensed data analysis are presented in this previous study (**41)**, notably for accounting
327 for uncertainty in data, guiding and informing the expert's decisions, and incorporating image
328 interpretation expertise and multiple data sources. The expert system was developed and operated
329 in the Google Earth Engine (GEE) geospatial cloud computing platform (**22).**

330

331 The mapping method includes four main steps described hereafter: (i) single-date multi-spectral
332 classification into three classes, (ii) analysis of trajectory of changes using the temporal information
333 and production of a 'transition' map (with seven classes) (**Figs. 1 and 2,** figs. S2 to S7), (iii)
334 identification of sub-classes of transition based on ancillary datasets (see Supplementary Text on
335 Ancillary datasets) and visual interpretation, (iv) production of annual change maps (fig. S1).

336

337 In the first step, each image of the Landsat archive was analysed on a single-date basis (through a
338 multi-spectral classification), whereas previous large-scale studies used annual syntheses or intra-
339 annual statistics such as the mean and standard deviation of available Landsat observations (**44-50**).
340 Classification of individual images is challenging but presents three main advantages: it allows (i)
341 to capture the disturbance events that are visible only over a short period from space, such as

342 logging activities, (ii) to record the precise timing of the disturbances and the number of *disruption*
343 *observations,* and (iii) to detect the disturbance at an early stage, i.e. even if the disturbance is
344 starting at the end of the year, it is detected and counted as a disturbance for this year whereas other
345 approaches notably based on composites will detect the disturbance with a delay of one year.
346 A *disruption observation* is defined here as an absence of tree foliage cover within a 0.09 ha size
347 Landsat pixel. The number of *disruption observations* constitutes a proxy of disturbance intensity.
348 Each pixel within a Landsat image was initially assigned through single-date multi-spectral
349 classification to one of three following classes: (i) *potential moist forest cover*, (ii) *potential*
350 *disruption*, and (iii) *invalid observation* (cloud, cloud shadow, haze and sensor issue).
351
352 The temporal sequence of classes (i) and (ii) was then used to determine the seven transition classes,
353 described in the second step of the mapping approach. However, not all pixels could be
354 unambiguously spectrally assigned to one of the three single-date classes because the multi-spectral
355 cluster hulls of such classes are overlapping in the multidimensional feature-space. In cases of
356 spectral confusion, evidential reasoning was used to guide class assignment by taking into
357 consideration the temporal trajectory of single-date classifications, as spectral overlap between land
358 cover types may occur only at specific periods of the year. For instance, pixels covered by
359 deciduous forests, grassland or agriculture, may behave – from a spectral point of view – as
360 *potential moist forest cover* during the humid seasons and as *potential disruptions* during the dry
361 seasons, and, consequently, can be assigned to the *other land cover* transition class. Disturbed moist
362 forests (degraded or deforested) are appearing as *potential moist forest cover* at the start of the
363 archive and as *potential disruption* assignments later.
364
365 For the three initial classes (*potential moist forest cover*, *potential disruption*, and *invalid*
366 *observation*), multispectral clusters were defined first by establishing a spectral library capturing

the spectral signatures of the land cover types and atmosphere perturbations that are present over the pan-tropical belt and targeted for these three classes : (i) moist forest types, (ii) deciduous forest, logged areas, savannah, bare soil, irrigated and non-irrigated cropland, evergreen shrubland and water (for the *potential disruption* class) and (iii) clouds, haze, cloud shadows (for the *invalid observations*). A total sample of 38 326 sampled pixels belonging to 1 512 Landsat scenes (L5, L7 and L8), were labelled through visual interpretation. The HSV (*hue, saturation, value*) transformation of the spectral bands - well adapted for satellite image analysis (**41, 52**) - were used to complement the spectral library. These components were computed using a standard transformation (**52**) for the following Landsat band combination: short-wave infrared (SWIR2), near infrared (NIR) and red. The stability of *hue* to the impacts of atmospheric effect is particularly desirable for identifying *potential disruption* in the humid tropics. The sensitivity of *saturation* and *value* to atmospheric variability is mainly used to detect *invalid* observations (haze). *Value* is particularly useful for identifying cloud shadows. The thermal infrared band (TIR) was relevant to detect *invalid* observations (clouds, haze) and bare soil, and the Normalized Difference Water Index (NDWI) to identify irrigated areas. The information held in the spectral library was analyzed through visual analytics to extract equations describing class cluster hulls in the multidimensional feature-space (fig. S17). An exploratory data analysis tool designed in a previous study (**41**) was used to support the interactive analysis.

In the second step of the mapping approach, the temporal sequence of single-date classifications at pixel scale was analysed to first determine the initial extent of the TMF domain and then to identify the change trajectories from this initial forest extent (fig. S2). Long-term changes cannot be determined uniformly for the entire pan-tropical region because the observation record varies (see Data), e.g. the first year of observation (fig. S18) is c. 1982 for Brazil and c. 2000 along the Gulf of Guinea. We have addressed this geographic and temporal discontinuities of the Landsat

392 archive by determining at the pixel level (i) a reference initial period (baseline) for mapping the
393 initial TMF extent and (ii) a monitoring period for detecting the changes. The data gaps at the
394 beginning of the archive were tackled by requiring a minimum period of four years with a minimum
395 of three valid observations per year or a minimum of five years with two valid observations per
396 year from the first available valid observation. Hence, lower is the annual number of valid
397 observations, higher is the length of the initial period. This minimizes the risk of inclusion of non-
398 forest cover types (such as agriculture) and deciduous forests in the baseline when there are few
399 valid observations over a short period. In addition, we have reduced the commission errors in our
400 baseline by accounting for possible confounding with commodities, wetlands, bamboo, and
401 deciduous forest (see Supplementary Text on ancillary datasets and specific tropical forest types).
402 From our initial TMF extent, we identified seven main transition classes (fig. S2) which are defined
403 thereafter. The first year of the monitoring period (that follows the initial period) is represented at
404 fig. S18; it starts at the earliest in year 1987 (mostly for South-America) and, for very limited cases,
405 at the latest in 2016 (e.g. Gabon).
406
407 Although no ecosystem may be considered truly undisturbed, because some degree of human
408 impact is present everywhere (**54**), we define the undisturbed moist forests (class 1) as tropical
409 moist (evergreen or semi-evergreen) forest coverage without any disturbance (degradation or
410 deforestation) observed over the Landsat historical record (see Section on the Study area and forest
411 types). Our TMF baseline may include old forest regrowth (old secondary forests) or previously
412 degraded forests forest as the Landsat observation period is too short to discriminate never-cut
413 primary forest from second growth naturally recovered forest older than the observation period.
414 This class includes two sub-classes of bamboo-dominated forest (class 1a) and undisturbed
415 mangrove (class 1b).

A *deforested land* (class 2) is defined as a permanent conversion from moist forest cover to another land cover whereas a *degraded forest* (class 3) is defined as a moist forest cover where disturbances were observed over a short time period. Here we assumed that the duration of the disturbance (and consequently the period over which we detect the disturbance with satellite imagery) is a proxy of the disturbance impact, i.e. higher is the duration of the detected disturbance, higher is the impact on the forest, and higher is the risk to have a permanent conversion of the TMF. By considering short-term disturbances we include logging activities, fires and natural damaging events such as wind breaks and extreme dryness periods. Hence, we are getting closer to the most commonly accepted definition of the degradation (**54**) that considers a loss of productivity, a loss of biodiversity, unusual disturbances (droughts, blowdown), and a reduction of carbon storage.

The threshold applied on the duration parameter used to separate *degraded forests* from *deforested land* is based on our knowledge of the impacts of human activities and of natural or human-induced events such as fires. We identified empirically two levels of degradation: (class 3a) degradation with short-duration impacts (observed within a 1-year maximum duration), which includes the majority of logging activities, natural events and light fires, and (class 3b) degradation with long-duration impacts (between one and 2.5 years) which mainly corresponds to strong fires (burned forests). Most of the degradation (50%) are observed over less than six-month durations (fig. S19). All disturbance events for which the impacts were observed over more than 2.5 years (900 days) were considered as deforestation processes, with 68% of such deforestation events observed over more than five years. When a deforestation process is not followed by a regrowth period at least over the last 3 years, it is considered as a *Deforested land*. Deforested land are also characterized by the recurrence of disruptions, i.e. the ratio between the number of years with at least one disruption observation and the total number of years between the first and last disruption observations. This information allowed to discriminate deforestation without prior degradation from deforestation occurring after degradation, the second one having a lower recurrence due to the

441 period without any disruption between the degradation and deforestation phases (see
442 Supplementary Text on annual change dataset).
443 *For the recent degradation and deforestation* (class 4) that initiated in the last three years (after
444 year 2016) and that cannot yet be attributed to a long-term conversion to a non-forest cover, owing
445 to the limited historical period of observation, specific rules were applied. Within this class, we
446 separated degradation from deforestation, by taking a duration of minimum 366 days for the years
447 2017-2018 and a threshold of 10 disruptions for the last year (2019) to consider a *deforested land*.
448 A *forest regrowth* (class 5) is a two-phase transition from moist forest to (i) deforested land and
449 then (ii) vegetative regrowth. A minimum 3-years duration of permanent moist forest cover
450 presence is needed to classify a pixel as forest regrowth (to avoid confusion with agriculture).
451 The *other land cover* (class 6) includes savannah, deciduous forest, agriculture, evergreen
452 shrubland and non-vegetated cover.
453 Finally, the *Vegetation regrowth (class 7)* consists of a transition from other land cover to
454 vegetation regrowth and includes two sub-classes of vegetation regrowth according to the age of
455 regrowth (between 3 and 10 years, and between 10 and 20 years) and a transition class from water
456 to vegetation regrowth.
457
458 The third mapping step allowed to identify three sub-classes from the *deforested land* class. We
459 geographically assigned deforestation to the conversion from TMF to tree plantations - mainly oil
460 palm and rubber (class 2a), water surface (discriminating permanent and seasonal water)- mainly
461 due to new dams (class 2b), and other land cover - agriculture, infrastructures, etc. (class 2c) using
462 ancillary spatial datasets completed by visual interpretation of high-resolution (HR) imagery (see
463 Supplementary Text on ancillary data). Finally, we have re-assigned disturbances when detected
464 within two geographically specific tropical forest formations: (i) the bamboo dominated forest, and

(ii) the semi-deciduous transition tropical forest (Supplementary Text on specific tropical forest formations).

Each disturbed pixel (degraded forest, deforested land, or forest regrowth) is characterized by the timing and intensity of the observed disruption events. The start and end dates of the disturbance allows identifying in particular the timing of creation of new roads or of logging activities and the age of forest regrowth or degraded forests. Three decadal periods have been used in the transition map to identify age sub-classes of degradation and forest regrowth: (i) before 2000, (ii) within 2000-2009 and (iii) within 2010-2019. The number of annual disruption observations combined with the duration, can be used as a proxy for the disturbance intensity and impact level.

In the last mapping step, we created a collection of 30 maps providing the spatial extent of the TMF and disturbance classes on a yearly basis, from 1990 to 2019, using dedicated decision rules (see Supplementary Text on the annual change dataset and thematic maps). These maps were used in our annual trend analysis -described in next subsection- to document the annual disturbances over the full period, with ten classes of transition for each annual statistic (**Figs. 3 and 4**, figs. S1 and S11): (i) degradation that occurs before deforestation, (iii) short-duration degradation not followed by deforestation, (iv) long-duration degradation not followed by deforestation, (v) direct deforestation (without prior degradation) not followed by forest regrowth, (vi) direct deforestation followed by forest regrowth, (viii) deforestation after degradation followed by forest regrowth, (viii) deforestation after degradation not followed by regrowth, (ix) forest conversion to water bodies and (x) forest conversion to tree plantations. The associated metadata information on invalid observations within the forest domain and the proportion of invalid observations over the forest domain area were also documented.

In order to produce a more conservative map of undisturbed forests by excluding potential missed areas impacted by logging activities, we created a disturbance buffer zone using a threshold distance of 120 m around disturbed pixels. This distance corresponds to the average observed distance between two logging desks (landing) and is consistent with the distances used in previous studies for assessing intact forests (**15**).

Trend analysis

The areas of TMF and disturbance classes are reported yearly and at 5-year intervals between 1990 and 2019, by country, subregion and continent (**Tables 1, 2, and 3**, **Figs. 3 and 4** and fig. S11, Supplementary Text on Trend analysis), using the country limits from the Global Administrative Unit Layers dataset from the FAO (**53**). Area measurements were also computed for 1° × 1° cells of a systematic latitude–longitude grid in order to delineate hotspot areas of deforestation and degradation for the three decades (**Fig. 5**). For the three most recent years of the considered period (i.e. for 2017-2019), the proportions of disturbance types (degradation followed by deforestation, degradation not followed by deforestation and direct deforestation) were calibrated with historical proportions (2005-2014) of the three types of disturbances.

For countries with moist forest areas larger than 5 million ha in 1990 (i.e. for 32 countries), and for all sub regions, we analyzed the temporal dynamics of annual changes from 1990 to 2019 (fig. S11 and Supplementary Text on trend analysis).

Validation

The performance of our classifier was assessed in term of errors of omission and commission at the pixel scale and the uncertainties in the area estimates derived from the transition map were quantified (see Supplementary Text on the validation). A stratified systematic sampling scheme was used to create a reference dataset of 5 250 sample plots of 3 × 3 pixels (0.81 ha plot size) (fig.

S8). For each sample plot, Landsat images at several dates were visually interpreted, together with the most recent HR images available from the Digital Globe or Bing collections, to create the reference dataset. The dates of the Landsat images to be interpreted were selected to optimize the assessment of the performance of our classifier as follows (fig. S9) ; (i) at least one random date within three successive key periods to verify the consistency of the temporal sequencing and the classifier performance across the main sensors (L5, L7 and L8), (ii) for the disturbed classes, the two dates corresponding to the first and last *disruption observations* were selected to assess the commission errors, and (iii) for the undisturbed forest class, at least one random date during the Global Forest Change (GFC) loss year (if existing) to assess omission errors. It resulted into the interpretation of two to four Landsat images for each sample plot, with a total of 14 295 images.

The user, producer and overall accuracies, the confidence intervals of the estimated accuracies and the corrected estimates of undisturbed and disturbed forest areas with a 95% confidence interval on this estimation were computed in accordance with latest statistical good practices (**26**). The performance of our disturbance detection results into 9.4% omissions, 8.1% false detections and 91.4% overall accuracy (tables S2 and S3). In addition, the uncertainties of area estimates (forest cover and changes) have been assessed from a sample of 5119 reference plots. This accuracy assessment shows that a direct area measurement from the forest cover maps underestimates the forest area changes by 11.8% (representing 38.4 million ha, with 15 million ha confidence interval at 95%) (tables S4 and S5).

Comparison with the Global Forest Change (GFC) dataset

We compared our transition classes with the GFC dataset (**24**) for the TMF domain (undisturbed and degraded forest) in 2000 and over the period 2001-2019, which is the common period between the two products.

We synthesized the GFC multiannual product into four classes of forest cover changes from the combination of the GFC annual layers of tree cover loss and gain over the period 2001-2019: (i) unchanged (no loss, no gain), (ii) at least one loss but no gain, (iii) at least one gain but no loss and (iv) at least one loss and one gain. A new version of the transition map with eight classes was created (through the combination with annual maps) to characterize the disturbances that occurred between 2001 and 2019: (i) undisturbed forest (at the end of 2019), (ii) old degradation or regrowth (initiated before 2001), (iii) old deforestation (before 2001), (iv) degradation initiated between 2001 and 2019, (v) direct deforestation initiated between 2001 and 2019, (vi) deforestation that follows a degradation and initiated between 2001 and 2019, (vii) regrowth initiated from 2001 (viii) other land cover.

A matrix of correspondences between the synthesized GFC map (four classes) and our reclassified transition map (eight classes) was then produced for each continent and for the pan-tropical region, where area estimates are compared (table S1). This comparison shows that our annual change dataset depicts 138.9 million ha of forest disturbances along the periods 2001-2019 that are not depicted in the GFC map (representing 59% of the total area of our disturbances). This finding is corroborated by previous studies (**33, 31**). In addition, 17.6 million ha and 3.2 million ha are depicted as a GFC loss whereas it is classified as old deforestation and degradation respectively (before 2001) in our TMF dataset. Amongst the disturbances that are not depicted by GFC, the highest disagreements concern the gradual processes such the degradation, the forest regrowth classes, and the deforestation that follows a degradation for which 75%, 67% and 59% respectively of our depicted areas are missing on the GFC map, whereas our direct deforestation class shows a good correspondence with the GFC map (60%). The disagreement between our dataset and the GFC map is even higher for the changes within the mangroves with 83% difference. Mangroves are a key ecosystem within the TMF. We also observed a lower agreement for the disturbance classes in Africa (38% of our disturbances are depicted by GFC) compared to other continents (40.9% and

565 43.3% for Asia and Latin America respectively). A higher underestimation of GFC loss in Africa
566 compared to other continents has also been observed by Tyukavina et al. (**31**) using a sample-based
567 analysis.
568
569 We observe higher discrepancies between GFC and our study for shorter and lower intensity events,
570 i.e. (i) the average duration for the disturbances detected only by our approach is 6.7 years compared
571 to 9.4 years for the disturbances captured by both approaches, and (ii) the average intensity (or total
572 number of disruptions detected for each disturbance) for the disturbances detected only by our
573 approach is 9.9 compared to 32.6 for the disturbances captured by both approaches.
574
575 The evolution of the discrepancies over time shows major differences between the period (2001-
576 2010) where our annual change dataset depicts 61.4% more deforested areas, and the last decade
577 (2010-2019) where GFC losses include all our deforestation areas and 5.7% of our degradation
578 areas (**Table 4 and Fig. 4**). This change in the last decade has also been observed in another study
579 (**56**) and can be explained (i) by the differences of processing applied by GFC team before and after
580 the year 2011 (https://earthenginepartners.appspot.com/science-2013-global-
581 forest/download_v1.3.html), and (ii) by the inclusion of burned areas in the GFC loss (particularly
582 for the dry period of 2015-2016) that are mainly classified as degradation in our TMF dataset.
583
584 ***Projection of future forest cover***
585 Temporal projections of future forest cover are provided for (i) undisturbed forest area and (ii) total
586 forest area (undisturbed and degraded forests) per country (fig. S12. and table S8). We considered
587 that the annual disturbed areas followed an independent log-normal distribution for each country,
588 and we used a modified version of the Cox method to estimate the mean and the 95% confidence
589 interval (**58**) of the distribution. We used these estimates on the last 10 years (period 2010-2019) to

project disturbances over the period 2020-2050 under a business-as-usual scenario. Several metrics, with their uncertainties, have been produced: (i) forest area at the end of 2050, (ii) percentage of remaining forest area at the end of 2050 compared with forest area at the end of 2019 and (iii) year corresponding to full disappearance of forest cover.

Known limitations and future improvements

Disturbances that affect less than the full pixel area (0.09 ha size), e.g. the removal of a single tree, are generally not included in our results because the impact of the spectral values of the pixel are not strong enough to be detected. However, in specific cases, where the impact on the forest canopy cover modifies significantly the spectral values within a single pixel, e.g. the opening of a narrow logging road (< 10 m wide) or the removal of several big trees, our approach can detect such disturbances.

We have addressed the geographic and temporal discontinuities of the Landsat archive (see Data and Mapping method) by determining at the pixel level (i) an initial period (baseline) of minimum four years (increasing when the annual number of valid observations is low) for mapping the initial TMF extent and (ii) a monitoring period for detecting the changes. This minimizes the risk of inclusion of non-forest cover types (such as agriculture) and deciduous forests in the baseline when there are few valid observations over a short period. This risk has been under-estimated by previous studies that did not use a long period of analysis and did not accounted for the number of valid observations.

The accuracy of the disturbance detections has been assessed in the validation exercise (see Validation section and Supplementary Text on the validation). The assignment of the disturbance types at any location improves as the number of valid observations increases. The meta-

615 information documents (i) the annual number of valid observations (ii) the first year of valid
616 observation (fig. S15) and (iii) the start year of the monitoring period (fig. S18) at each pixel
617 location. This meta-information (in particular the number of valid observations) can be
618 considered as a proxy measure of confidence. Hence our estimates of changes in the regions
619 where the total number of valid observations is particularly low and/or the start year of the
620 monitoring period is late (figs. S14, S15, S18ra), e.g. Gabon, Salomon Islands, La Reunion,
621 should be considered with lower confidence. However, considering the geographic completeness
622 of Landsat-8 coverage after year 2013 there is high confidence for the contemporary reported
623 estimates.
624
625 Short-duration events are likely to be underestimated for regions with geographic and temporal
626 discontinuities in the Landsat archive and/or with gaps caused by persistent cloud cover. This is the
627 case of Africa which is poorly covered by Landsat acquisitions before year 2000 (fig. S16). In order
628 to provide a more conservative estimate of the remaining undisturbed forested areas, we also
629 produced another estimate of undisturbed forested areas using a buffer zone with a threshold
630 distance of 120 m from the detected disturbed pixels to exclude the potentially edge-affected forest
631 areas. Further contextual spatial analysis would be needed to better estimate the characteristics of
632 fragmented areas.
633
634 For the first time at pan tropical scale, a fine spatial resolution and annual frequency, detailed
635 information on the historical forest area changes within the plantation concessions of oil palm and
636 rubber are provided through to the combination of ancillary information and dedicated visual
637 interpretation (see Supplementary Text on ancillary datasets). Although some confusion between
638 forests and old plantations may remain (in particular for plantations that are not included in the
639 ancillary database of concessions or that cannot be easily identified visually on satellite imagery

640 from a regular geometrical shape), such errors are expected to be limited due to the consideration
641 of (i) a minimum duration for the initial period and (ii) a long observation period. Classes of tree
642 plantations do not include all commodities such as coffee, tea and coconut, that are detected as
643 deforested land (if initially TMF and converted in commodity during the monitoring period) or
644 other land cover (if the concession was already established during the initial period).
645
646 Some isolated commission errors may remain in the bamboo-dominated TMF, wetlands and semi-
647 deciduous forests as reference data were available on restricted areas (Supplementary Text on
648 specific tropical forest types). These will be continuously improved as the reference information
649 layers improve and based on the feedback of users and national authorities.
650
651 The L7 SLC-off issue may introduce some spatial inconsistencies owing to a higher number of
652 valid observations outside the SLC-off stripes which allows more disruptions to be captured and
653 leads – potentially - to a different transition class.
654
655 Efforts have been done to classify disturbances based on their characteristics (timing, recurrence
656 and sequence) in order to fit to the land cover use. However, all the metrics used in this study are
657 made freely available to the end-user to possibly apply different decision rules that would better fit
658 to the specific user needs and constraints, e.g. threshold applied to discriminate deforestation from
659 degradation may be different according to the selected definition of the degradation.
660
661 This approach can be automatically applied to future Landsat data (from 2020) and is intended
662 to be adapted to Sentinel 2 data (available since 2015) towards a monitoring of tropical moist
663 forests with higher temporal frequency and finer spatial resolution.
664

665 **SUPPLEMENTARY MATERIALS**

666 This file contains Supplementary Text on ancillary data, on specific tropical forest formations, on
667 the transition map, on the annual change dataset, on the validation, on the trend analysis,
668 supplementary references, supplementary figures and supplementary tables.

669

670 **REFERENCES**

671 1. Gibson, L., Lee, T. M., Koh, L. P., Brook, B. W., Gardner, T. A., Barlow, J., Peres, C. A.,
672 Bradshaw, C. J. A., Laurance, W. F., Lovejoy, T. E., Sodhi, N. S. Primary forests are
673 irreplaceable for sustaining tropical biodiversity. *Nature* **478**, 378–381 (2011).
674 doi:10.1038/nature10425

675 **2.** Watson, J. E. M. , Evans, T., Venter, O., Williams, B., Tulloch, A., Stewart, C., Thompson, I.,
676 Ray, J. C., Murray, K., Salazar, A., McAlpine, C., Potapov, P., Walston, J., Robinson, ., J. G.,
677 Painter, M., Wilkie, D., Filardi, C., Laurance, W. F., Houghton, R. A., Maxwell, S., Grantham,
678 H., Samper, C., Wang, S., Laestadius, L., Runting, R. K., Silva-Chávez, G. A., Ervin, J.,
679 Lindenmayer, D. The exceptional value of intact forest ecosystems. *Nature Ecology &*
680 *Evolution* **2**, 599–610 (2018). Doi:10.1038/s41559-018-0490-x

681 3. Mackey, B., DellaSala, D. A., Kormos, C., Lindenmayer, D., Kumpel, N., Zimmerman, B.,
682 Hugh, S., Young, V., Foley, S., Arsenis, K., Watson, J. E. M. Policy options for the world's
683 primary forests in multilateral environmental agreements. *Conserv. Lett.* **8**, 139–147 (2015).
684 doi:10.1111/conl.12120

685 4. Luyssaert, S., Schulze, E.-D., Börner, A., Knohl, A., Hessenmöller, D., Law, B. E., Ciais, P.,
686 Grace, J. Old-growth forests as global carbon sinks. *Nature* **455**, 213–215 (2008).
687 doi:10.1038/nature07276

688 5. Aerts, R., Honnay, O. Forest restoration, biodiversity and ecosystem functioning. *BMC*
689 *Ecology*, **11**, 1-10 (2011). doi:10.1186/1472-6785-11-29

690 6. Alkama, R., Cescati, A. Biophysical climate impacts of recent changes in global forest cover.
691 *Science* **351**, 600-604 (2016). doi:10.1126/science.aac8083.
692 7. Grassi, G., House, J., Dentener, F., Federici, S., den Elzen, M., Penman, J. Key role of forests
693 in meeting climate targets but science needed for credible mitigation. *Nature Climate Change*
694 **7**, 220–226 (2017). doi:10.1038/NCLIMATE3227
695 8. Barlow, J., Lennox, G.D., Ferreira, J., Berenguer, E., Lees, A. C., Mac Nally, R., Thomson, J.
696 R., Frosini de Barros Ferraz, S., Louzada, J., Fonseca Oliveira, V. H., Parry, L., Ribeiro de
697 Castro Solar, R., Vieira, I. C. G., Aragão, L. E. O. C., Anzolin Begotti, R., Braga, R. F., Moreira
698 Cardoso, T., Cosme de Oliveira Jr, R., Souza Jr, C. M., Moura, N. G., Serra Nunes, S., Victor
699 Siqueira, J., Pardini, R., Silveira, J. M., Vaz-de-Mello, F. Z., Carlo Stulpen Veiga, R., Venturier,
700 A., Gardner, T. A. Anthropogenic disturbance in tropical forests can double biodiversity loss
701 from deforestation. *Nature* **535**, 144-147 (2016). doi:10.1038/nature18326
702 9. Strona, G., Stringer, S. D., Vieilledent, G., Szantoi, Z., Garcia-Ulloa, J., Wich, S., Small room
703 for compromise between oil palm cultivation and primate conservation in Africa. *Proc. Natl.*
704 *Acad. Sci. U.S.A.*, **115**: 8811–8816 (2018). doi: 10.1073/pnas.1804775115
705 10. Mitchard, E.T.A. The tropical forest carbon cycle and climate change, *Nature,* **559**, 527-534
706 (2018).
707 11. Laurance, W. F., Goosem, M., Laurance, S. G. W. Impacts of roads and linear clearings on
708 tropical forests. *Trends Ecol. Evol.* **24**:659–669 (2009). doi:10.1016/j.tree.2009.06.009.
709 12. Brienen, R., Phillips, O., Feldpausch, T., Gloor, E., Baker, T., Lloyd, J., Lopez-Gonzalez, G.,
710 Monteagudo-Mendoza, A., Malhi, Y., Lewis, S. *et al.,* Long-term decline of the Amazon carbon
711 sink Nature, *Nature Publishing Group*, **519**, 344-348, (2015).
712 13. Baccini, A., Walker, W., Carvalho, L., Farina, M., Sulla-Menashe, D., Houghton, R. A. Tropical
713 forests are a net carbon source based on aboveground measurements of gain and loss. *Science*
714 **358**, 230–234 (2017). doi:10.1126/science.aam5962

14. Brinck, K., Fischer, R., Groeneveld, J., Lehmann, S., Dantas De Paula, M., Pütz, S., Sexton, J. O., Song, D., Huth, A. High resolution analysis of tropical forest fragmentation and its impact on the global carbon cycle. *Nat. Commun.* **8**, 14855 (2017). doi:10.1038/ncomms14855

15. Qie, L. , Lewis, S.L. , Sullivan, M.J.P., Lopez-Gonzalez, G., Pickavance, G.C., Sunderland, T., Ashton, P., Hubau, W., Abu Salim, K., Aiba, S-I., Banin, L.F., Berry, N., Brearley, F.Q., Burslem, D.F.R.P., Dančák, M., Davies, S.J., Fredriksson, G., Hamer, K.C., Hédl, R., Kho, L.K., Kitayama , K , Krisnawati , H , Lhota , S , Malhi , Y , *et al*. Long-term carbon sink in Borneo's forests halted by drought and vulnerable to edge effects. *Nat. Commun.* **8**, 1966 (2017) doi: 10.1038/s41467-017-01997-0

16. Pütz, S., Groeneveld, J., Henle, K., Knogge, C., Camargo Martensen, A., Metz, M., Metzger, J. P., Cezar Ribeiro, M., Dantas de Paula, M., Huth, A. Long-term carbon loss in fragmented Neotropical forests. *Nature Communications* **5**, 5037 (2014). doi:10.1038/ncomms6037

17. Fu, Z., Li, D., Hararuk, O., Schwalm, C., Luo, Y., Yan, L., Niu, S. Recovery time and state change of terrestrial carbon cycle after disturbance. *Environ. Res. Lett*. 12, 104004 (2017). doi:10.1088/1748-9326/aa8a5c

18. Olivero, J., Fa, J. E., Real, R., Márquez, A. L., Farfán, M. A., Vargas, J.M. et al. (2017). Recent loss of closed forests is associated with Ebola virus disease outbreaks. *Scientific Reports*, **7**, 14291. https://doi.org/10.1038/s41598-017-14727-9

19. Rulli, M.C., Santini, M., Hayman, D.T.S. and D'Odorico, P. (2017). The nexus between forest fragmentation in Africa and Ebola virus disease outbreaks. *Scientific Reports*, **7**, 41613. https://doi.org/10.1038/srep41613

20. MacDonald, A.J., and Mordecai, E.A., Amazon deforestation drives malaria transmission, and malaria burden reduces forest clearing. *PNAS*, 116, 22212-22218 (2019). https://doi.org/10.1073/pnas.1905315116

21. Potapov, P., Hansen, M.C., Laestadius, L., Turubanova, S., Yaroshenko, A., Thies, C., Smith, W., Zhuravleva, I., Komarova, A., Minnemeyer, S. et al. The last frontiers of wilderness: Tracking loss of intact forest landscapes from 2000 to 2013. *Sci. Adv.* **3**, (2017). doi:10.1126/sciadv.1600821

22. Gorelick, N., Hancher, M., Dixon, M., Ilyushchenko, S., Thau, D., Moore, R. Google Earth Engine: Planetary-scale geospatial analysis for everyone. *Remote Sens. Environ.* ***202***, 18–27 (2017). Doi:10.1016/j.rse.2017.06.031

23. Woodcock, C.E. , Allen, R., Anderson, M., Belward, A., Bindschadler, R., Cohen, W., Gao, F., Goward, S.N., Helder, D., Helmer, E., Nemani, R., Oreopoulos, L., Schott, J., Thenkabail, P.S., Vermote, E.F., Vogelmann, J., Wulder, M.A., Wynne, R. Free access to Landsat imagery. *Science* **320**, 1011 (2008). doi:10.1126/science.320.5879.1011a

24. Hansen, M. C., Potapov, P.V., Moore, R., Hancher, M., Turubanova, S.A., Tyukavina, A., Thau, D., Stehman, S.V., Goetz, S.J., Loveland, T.R. *et al*. High-resolution global maps of 21st-century forest cover change. *Science* ***342***, 850–853 (2013). Doi:10.1126/science.1244693

25. Kim, D.-H., Sexton, J. O., Noojipady, P., Huang, C., Anand, A., Channan, S., Feng, M., Townshend, J.R. Global, Landsat-based forest-cover change from 1990 to 2000. *Remote Sensing of Environment* **155**, 178-193 (2014). Doi:10.1016/j.rse.2014.08.017

26. Olofsson, P., Foody, G. M., Herold, M., Stehman, S. V., Woodcock, C. E., Wulder, M.A. Good practices for estimating area and assessing accuracy of land change. *Remote Sens. Environ*. **148**, 42–57 (2014).

27. Fonseca, M. G., Anderson, L.O., Arai, E., Shimabukuro, Y. E., Xaud, H. A. M., Xaud, M. R., Madani, N., Wagner, F. H., Aragão, L.E.O.C. Climatic and anthropogenic drivers of northern Amazon fires during the 2015/2016 El Niño event. *Ecological Applications* **27**, 2514-2527 (2017). Doi:10.1002/eap.1628

765 28. Aragão, L.E.O.C., Anderson, L.O., Fonseca, M.G., Rosan, T.M., Vedovato, L.B., Wagner, F.
766 H., Silva, C. V. J., Silva Junior, C. H. L., Arai, E., Aguiar, A. P., Barlow, J., Berenguer, E.,
767 Deeter, M. N., Domingues, L. G., Gatti, L., Gloor, M., Malhi, Y., Marengo, J.A., Miller, J.B.,
768 Phillips, O.L., Saatchi, S. 21st Century drought-related fires counteract the decline of Amazon
769 deforestation carbon emission. *Nature Communications* **9**,536 (2018).
770 29. Jiménez-Muñoz, J. C., Mattar, C., Barichivich, J., Santamaría-Artigas, A.,Takahashi, K., Malhi,
771 Y., Sobrino, J. A., van der Schrier, G. Record-breaking warming and extreme drought in the
772 Amazon rainforest during the course of El Niño 2015–2016. *Sci. Rep.* **6**, 33130 (2016) doi:
773 10.1038/srep33130 (2016).INPE PRODES
774 (http://www.obt.inpe.br/OBT/assuntos/programas/amazonia/prodes)
775 30. Keenan, R. J., Reams, G.A., Achard, F., de Freitas, J.V., Grainger, A., Lindquist, E., Dynamics
776 of global forest area: Results from the FAO Global Forest Resources Assessment 2015. Forest
777 Ecology and Management 352, 9-20 (2015). doi:10.1016/j.foreco.2015.06.014
778 31. Tyukavina, A., Baccini, A., Hansen, M.C., Potapov, P.V., Stehman, S.V., Houghton, R.A.,
779 Krylov, A.M., Turubanova, S., Goetz, S.J. Aboveground carbon loss in natural and managed
780 tropical forests from 2000 to 2012. *Environ. Res. Lett*. **10**, 074002 (2015). doi:10.1088/1748-
781 9326/10/7/074002
782 32. Achard, F., Beuchle, R., Mayaux, P., Stibig, H-J., Bodart, C., Brink, A., Carboni, S., Desclée,
783 B., Donnay, F., Eva, H.D., Lupi, A., Raši, R., Seliger, R., Simonetti, D. Determination of
784 tropical deforestation rates and related carbon losses from 1990 to 2010. *Glob. Chang. Biol.* **20**,
785 2540–2554 (2014). doi:10.1111/gcb.12605
786 33. Tropek, R., Sedláček, O., Beck, J., Keil, P., Musilová, Z., Šímová, I., Storch, D. Comment on
787 "High-resolution global maps of 21st-century forest cover change". Science 344, 981 (2014).

34. Finer, M., Novoa, S., Weisse, M. J., Petersen, R., Mascaro, J., Souto, T., Stearns, F., García Martinez R., Combating deforestation: From satellite to intervention. *Science* 360, 1303-1305 (2018). doi:10.1126/science.aat1203.

35. Whitmore, T.C. An introduction to tropical rain forests. Oxford: Clarendon (1990).

36. FAO, Global Ecological Zones for FAO forest reporting: 2010 Update (U.N. Food and Agriculture Organization, 2012). (http://www.fao.org/geonetwork/srv/en/main.home)

37. Wulder, M. A., Masek, J. G., Cohen, W. B., Loveland, T. R., Woodcock, C. E. Opening the archive: How free data has enabled the science and monitoring promise of Landsat. *Remote Sens. Environ*. **122**, 2–10 (2012). doi:10.1016/j.rse.2012.01.010

38. Markham, B. L., Storey, J. C., Williams, D. L., Irons, J. R. Landsat sensor performance: history and current status. *IEEE Transactions on Geoscience and Remote Sensing* **42**, 2691–2694 (2004).

39. Goward, S., Arvidson, T., Williams, D., Faundeen, J., Irons, J., Franks, S. Historical Record of Landsat Global Coverage Mission Operations, NSLRSDA, and International Cooperator Stations. *Photogrammetric Engineering & Remote Sensing* **72**, 1155–1169 (2006).

40. Chen, J., Zhu, X., Vogelmann, J.E., Gao, F., Jin, S. A simple and effective method for filling gaps in Landsat ETM+ SLC-off images. *Remote Sens. Environ*. **115**, 1053-1064 (2011). doi:10.1016/j.rse.2010.12.010

41. Pekel, J.-F., Cottam, A., Gorelick, N., Belward, A. S. High-resolution mapping of global surface water and its long-term changes. *Nature* **540**, 418-422 (2016). doi: 10.1038/nature20584

42. Keim, D. A. et al. in Visual Data Mining 76–90, http://kops.uni-konstanz.de/bitstream/handle/123456789/5631/Visual_Analytics_Scope_and_Challenges.pdf?sequence=1&isAllowed=y (Springer, 2008).

43. Yang, J.-B. & Xu, D. L. On the evidential reasoning algorithm for multiple attribute decision analysis under uncertainty. *IEEE Trans. Syst. Man Cybern. A* **32**, 289–304 (2002).

813 44. Roy, D. P., Ju, J., Kline, K., Scaramuzza, P.L., Kovalskyy, V., Hansen, M. C., Loveland, T.R,
814 Vermote, E., Zhang, C. Web-Enabled Landat Data (WELD): Landsat ETM+ composited
815 Mosaics of the Conterminous United States. *Remote Sens. Environ*. **114**, 35-49 (2010).
816 doi:10.1016/j.rse.2009.08.011
817 45. Potapov, P. V., Turubanova, S. A., Hansen, M. C., Adusei, B., Broich, M., Altstatt, A., Mane,
818 L., Justice, C.O. Quantifying forest cover loss in Democratic Republic of the Congo, 2000–
819 2010, with Landsat ETM+ data. *Remote Sens. Environ.* **122**, 106-116 (2012)
820 doi:10.1016/j.rse.2011.08.027
821 46. Margono, A., Turubanova, S., Zhuravleva, I., Potapov, P., Tyukavina, A., Baccini, A., Goetz,
822 S., Hansen, M. C. Mapping and monitoring deforestation and forest degradation in Sumatra
823 (Indonesia) using Landsat time series data sets from 1990 to 2010. *Environmental Research*
824 *Letters* **7,** 034010 (2012). doi:10.1088/1748-9326/7/3/034010
825 47. Griffiths, P., Kuemmerle, T., Baumann, M., Radeloff, V.C., Abrudan, I.V., Lieskovsky, J.,
826 Munteaunu, C., Ostapowicz, K., Hostert, P. Forest disturbances, forest recovery, and changes
827 in forest types across the Carpathian ecoregion from 1985 to 2010 based on Landsat Image
828 Composites. *Remote Sens. Environ*. **151**, 72-88 (2014). doi:101016/j.rse.2013.04.022
829 48. Potapov, P. V., Turubanova, S. A., Tyukavina, A., Krylov, A. M., McCarty, J. L., Radeloff, V.
830 C., Hansen, M. C. Eastern Europe's forest cover dynamics from 1985 to 2012 quantified from
831 the full Landsat archive. *Remote Sens. Environ*. **159**, 28-43 (2015).
832 doi:10.1016/j.rse.2014.11.027
833 49. Muller, H., Griffiths, P., Hostert, P. Long-term deforestation dynamics in the Brazilian Amazon
834 - Uncovering historic frontier development along the Cuiabá–Santarém highway. International
835 *Journal of Applied Earth Observation and Geoinformation* **44**, 61-69 (2016).
836 doi: 10.1016/j.jag.2015.07.005

50. Hermosilla, T., Wulder, M. A., White, J.C., Coops, N .C.,, Hobard, G. W. Updating Landsat time series of surface-reflectance composites and forest change products with new observations. *International Journal of Applied Earth Observation and Geoinformation* **63**, 104-111 (2017). doi: 10.1016/j.jag.2017.07.013

51. Pekel, J.-F. Vancutsem, C., Bastin, L., Clerici, M., Vanbogaert, E., Bartholomé, E., Defourny, P. A near real-time water surface detection method based on HSV transformation of MODIS multi-spectral time series data. *Remote Sens. Environ*. **140**, 704–716 (2014). doi.org/10.1016/j.rse.2013.10.008

52. Smith, A. R. Color gamut transform pairs. *Comput. Graph*. **12**, 12–19 (1978).

53. FAO, Global Administrative Unit Layers (GAUL) (http://www.fao.org/geonetwork/srv/en/main.home)

54. Sanderson, E. W., Jaiteh, M., Levy, M. A., Redford, K. H., Wannebo, A. V., Woolmer, G. The human footprint and the last of the wild. *Bioscience* **52**, 891–904 (2002). Doi:10.1641/0006-3568(2002)052

55. Thompson, I., Guariguata, M.R, Okabe, K., Bahamondez, C., Nasi, Heymell, R., Sabogal S., An Operational Framework for Defining and Monitoring Forest Degradation. *Ecology and* Society 18(2):20 (2013). doi: 10.5751/ES-05443-180220

56. Galiatsatos, N. Donoghue, D.N.M., Watt, P., Bholanath, P., Pickering, J., Hansen, M.C. and Mahmood, A.R.J. An Assessment of Global Forest Change Datasets for National Forest Monitoring and Reporting. *Remote Sens. **12**, 1790* (2020).

57. Turubanova, S., Potapov, A.V., Tyukavina, A., Hansen, M.C., Ongoing primary forest loss in Brazil, Democratic Republic of the Congo, and Indonesia, *Environ. Res. Lett*. **13**, (2018).

58. Olsson, U. Confidence intervals for the mean of a log-normal distribution. *Journal of Statistics Education* **13** (2005)

862 **ACKNOWLEDGMENTS**

863 The USGS and NASA provided the Landsat imagery. R. Moore and her team provided the Google
864 Earth Engine. Noel Gorelick, Mike Dixon, and Chris Herwig provided support in GEE.
865 Andrew Cottam provided support for the validation tool (adaptation from the water surface
866 validation tool). Andreas Langner, Hans-Jurgen Stibig, Rene Beuchle, Astrid Verhegghen, Hugh
867 Eva, Rosana Grecci, and Baudouin Desclee provided a useful feedback on the legend and products
868 in the framework of the ReCaREDD (Reinforcement of Capacities for REDD+) and
869 REDDCopernicus projects. We thank Alessandro Cescatti and Philippe Mayaux for reviewing
870 earlier versions of the manuscript.

871 This study was funded by the Directorate-General for Climate Action of the European Commission
872 (DG-CLIMA) in the framework of the *Roadless-For* pilot project (Making efficient use of EU
873 climate finance: Using roads as an early performance indicator for REDD+ projects).

874

875 **CONTRIBUTIONS**

876 CV was the principal investigator of this study. CV developed the expert system, implemented all
877 the steps and analyzed the results. The manuscript was prepared by CV and FA, with the
878 contributions of J-F.P., GV, JG, LA and RN. FA contributed to the analysis of the results. CV, FA
879 and JG developed together the validation method. J-F.P contributed to the development of the
880 expert system. GV realized the deforestation predictions, provided support with Python and gave a
881 useful feedback on the maps produced. SC realized the validation exercise and contributed to the
882 creation of the plantation database. DS gave a support for coding with GEE and Python. AM and
883 DS realized the website.

884

885

886

887 **FIGURES AND TABLES**

888 **Fig. 1.** Map of tropical moist forests remaining in January 2020 and disturbances observed during

889 the period 1990-2019. See legend in Fig. 2.

890

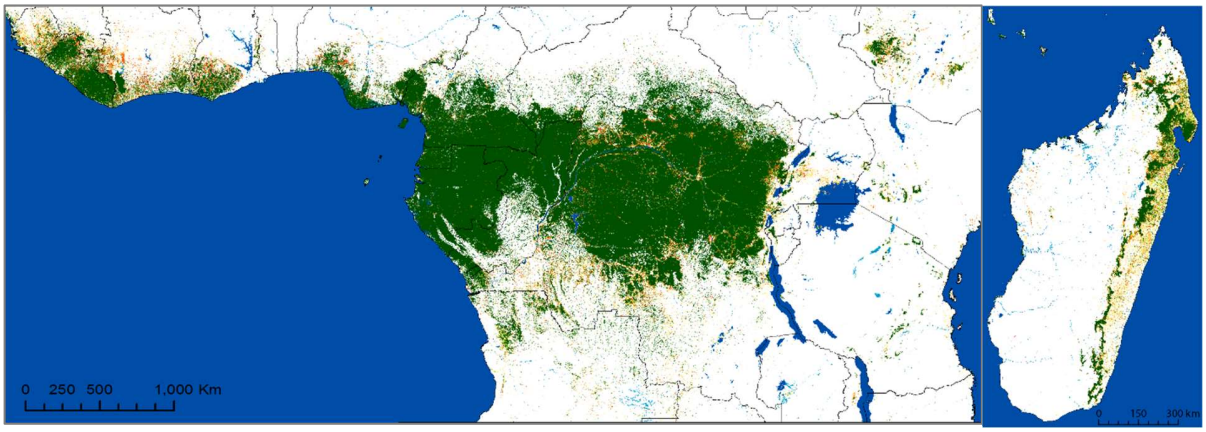

891

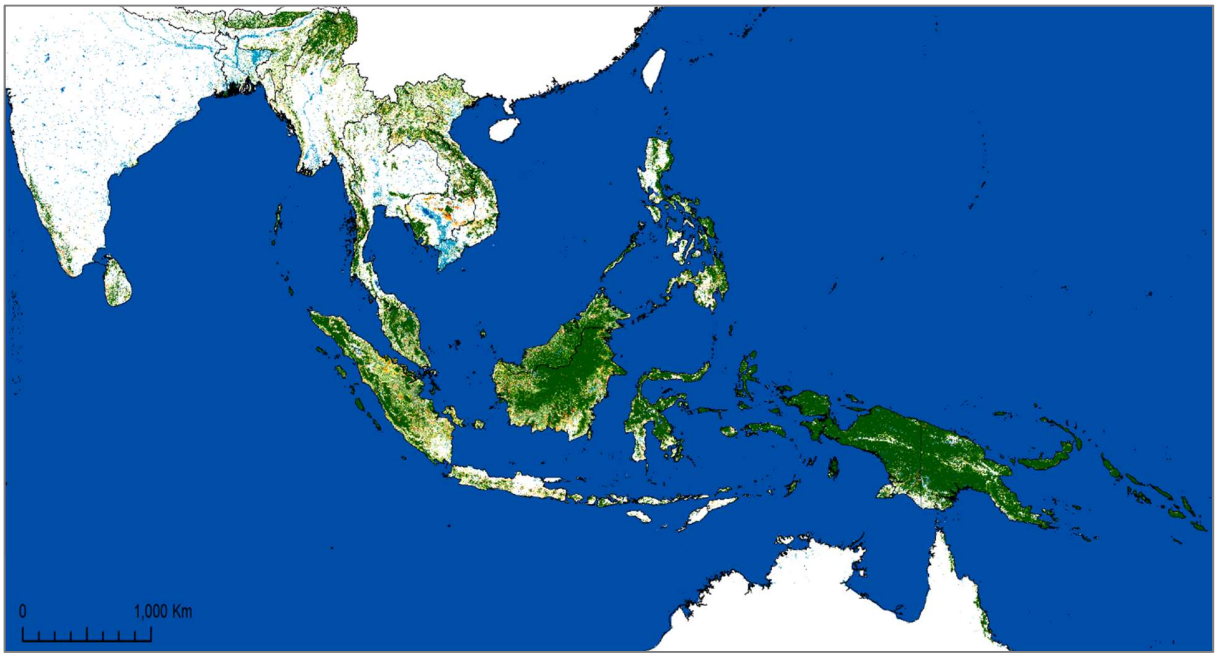

892

893

894

895

Fig. 2. Examples of patterns of forest cover disturbances (deforestation and degradation) during the period 1990-2019 : (A) Remaining Mangroves and the related changes in Guinea-Bissau (14.9˚W, 11.1˚N), (B) Fires in Mato-Grosso province of Brazil (53.8˚W, 13˚S), (C) Recent deforestation in Colombia (74.4˚W, 0.7˚N), (D) Logging in Mato-Grosso (54.5˚W, 12˚S), (E) Deforestation and degradation caused by the railway in Cameroon (13.4˚E, 5.8˚N) (F) Recent selective logging in Ouesso region of Republic of Congo (15.7˚E, 1.4˚N), (G) Deforestation for the creation of a dam in Malaysia (113.8˚E, 2.4˚S), (H) Massive deforestation in Cambodia (105.6˚E, 12.7˚N), and (I) Commodities in the Riau province of Indonesia (102˚E, 0.4˚N). The size of each box is 20 km × 20 km.

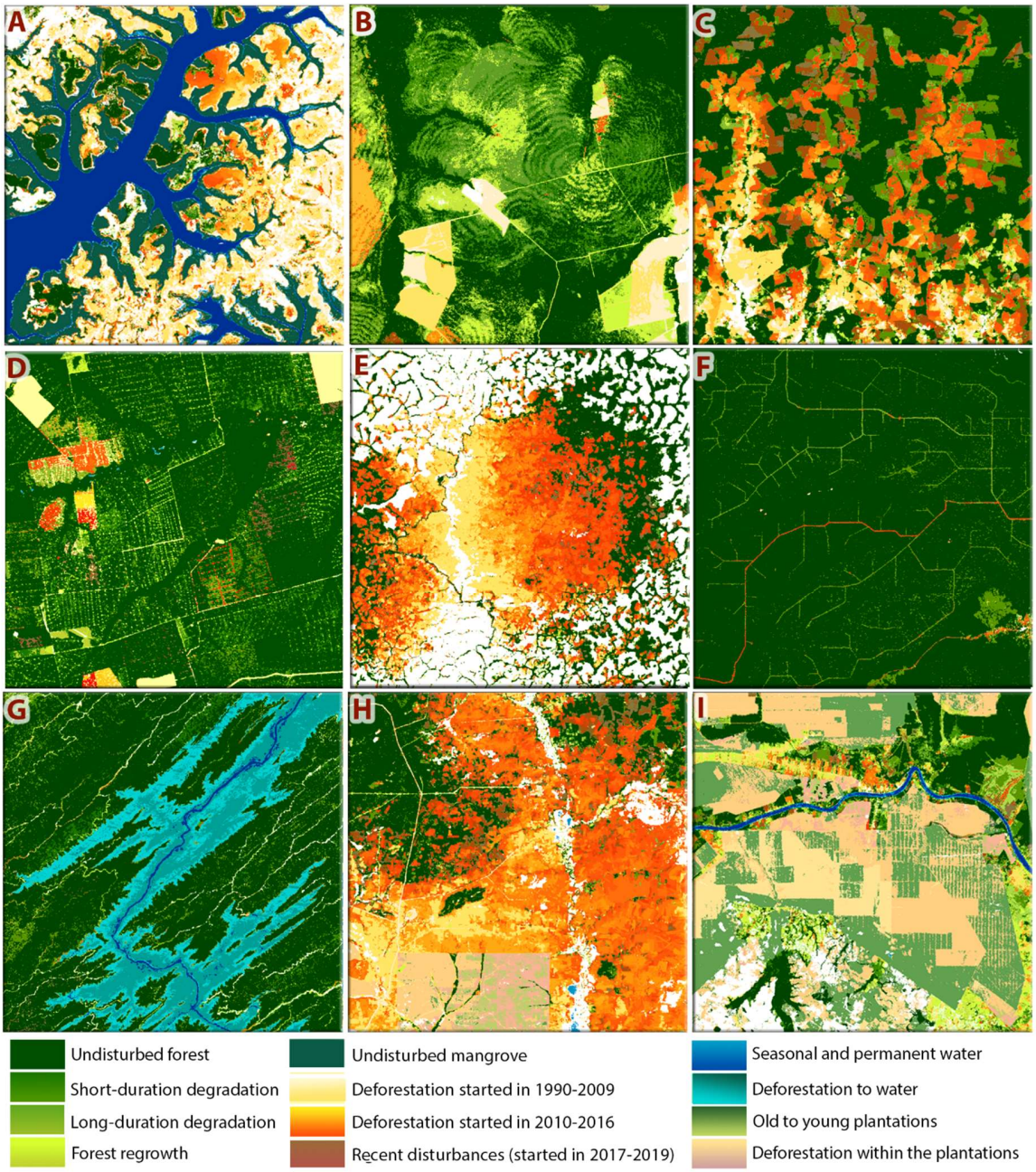

Fig. 3 Evolution of annual deforestation and degradation (A) over the last 25 years in South America, and (B) in continental South-East Asia regions, and (C) over the last 15 years in all regions.

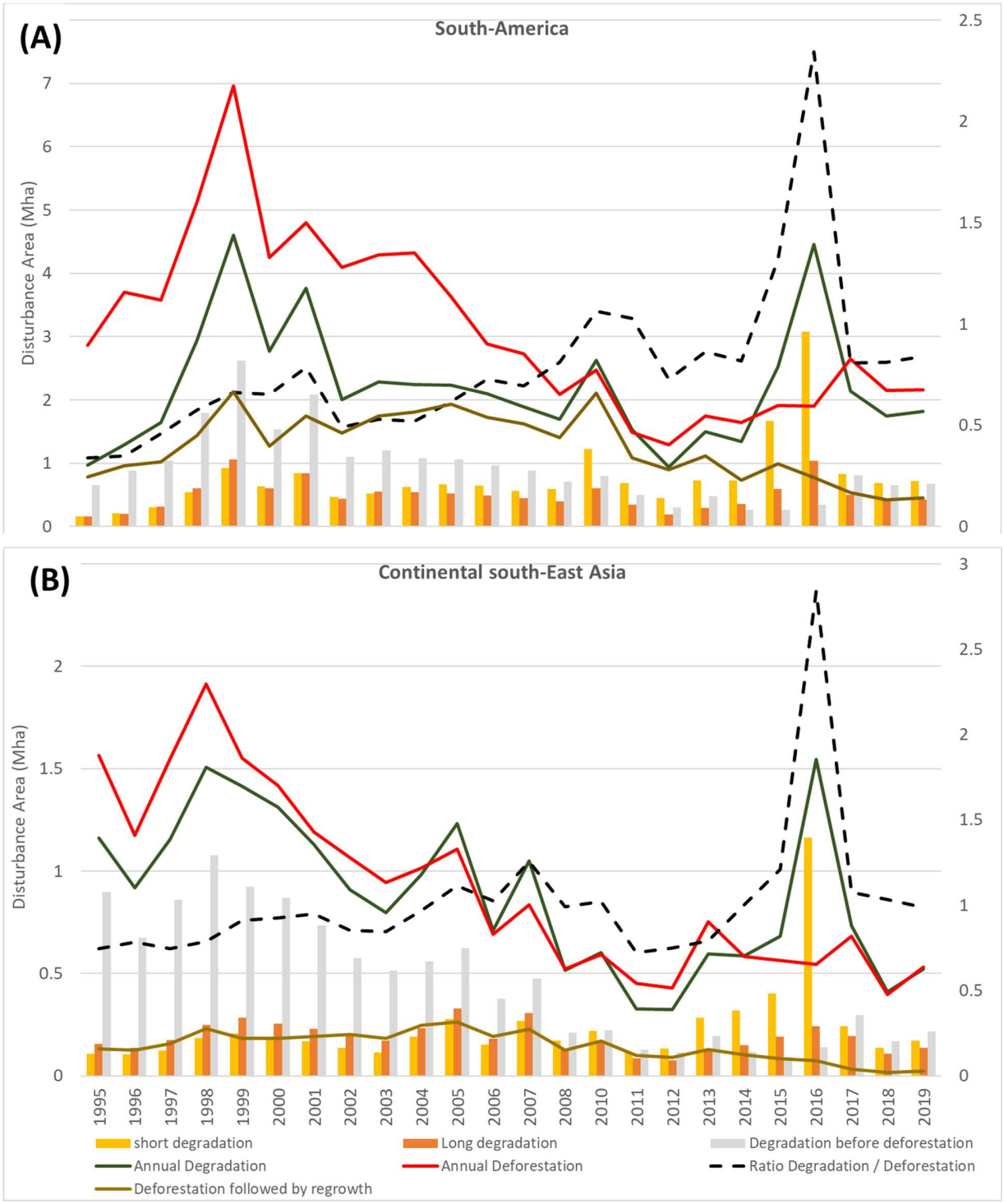

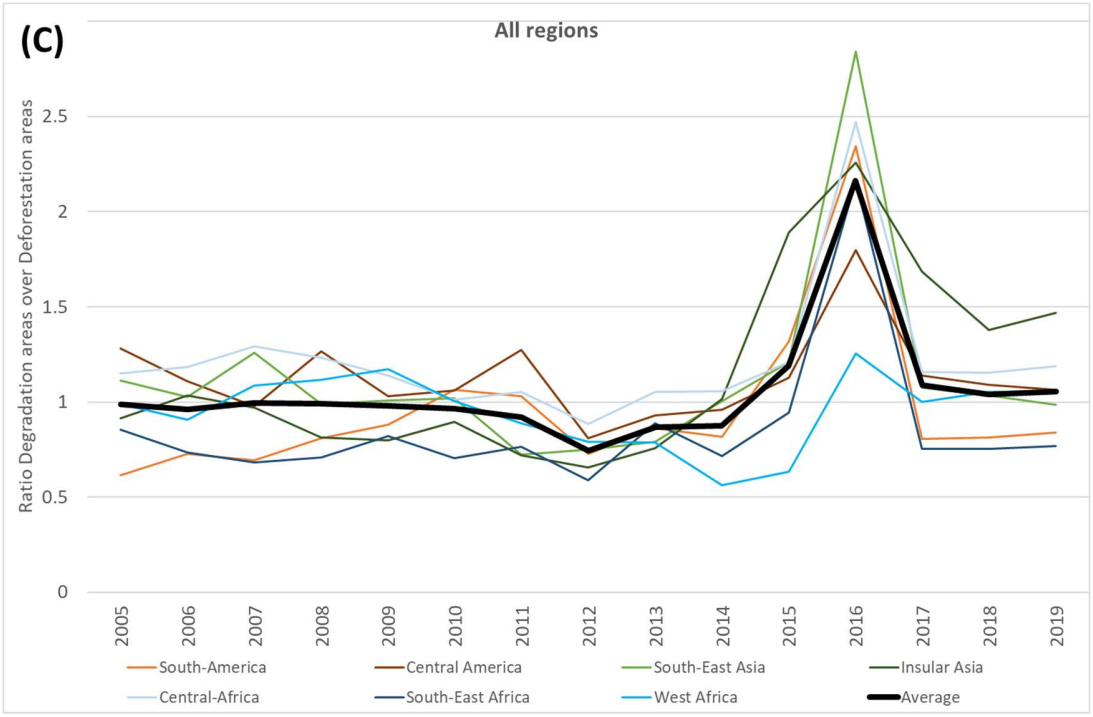

Fig. 4 Dynamics of annual disturbed areas from 2001 to 2019 for (A) the Amazônia Legal region of Brazil within the primary forest extent in 2000 from INPE and (B) Indonesia using the entire TMF extent (undisturbed and degraded) in 2000. (x-axis in years and y-axis in million ha) in comparison with GFC loss and the PRODES data for the Amazônia Legal region of Brazil. * The average proportions of disturbance types within total disturbances over the period 2005-2014 is used to distribute the disturbance types for years 2017 to 2019.

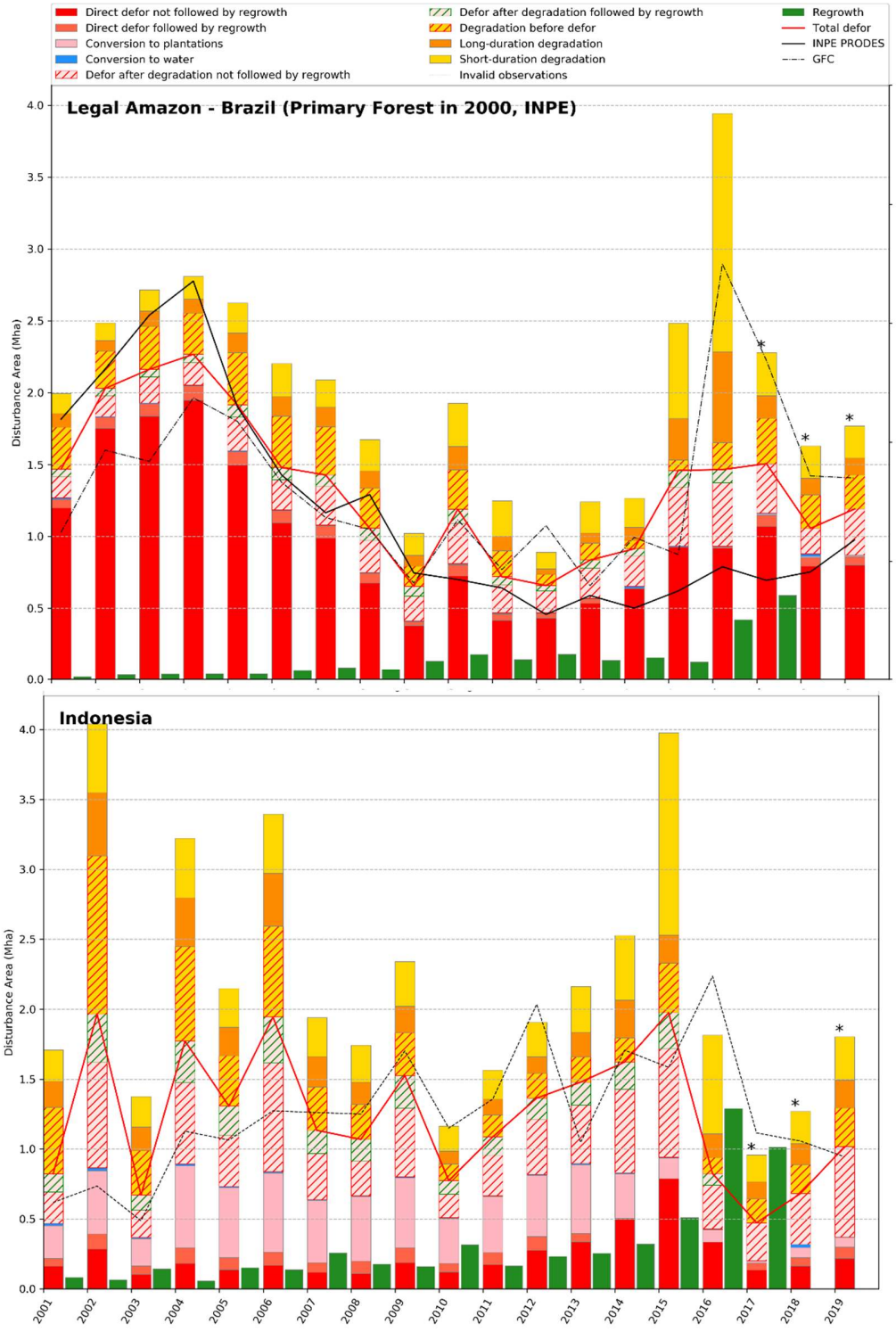

936 **Fig. 5** Evolution of hotspots of deforestation (A) and degradation (B) during the last three decades
937 (total deforested or degraded area per box of 1˚ latitude × 1˚ longitude size – scale in million ha).

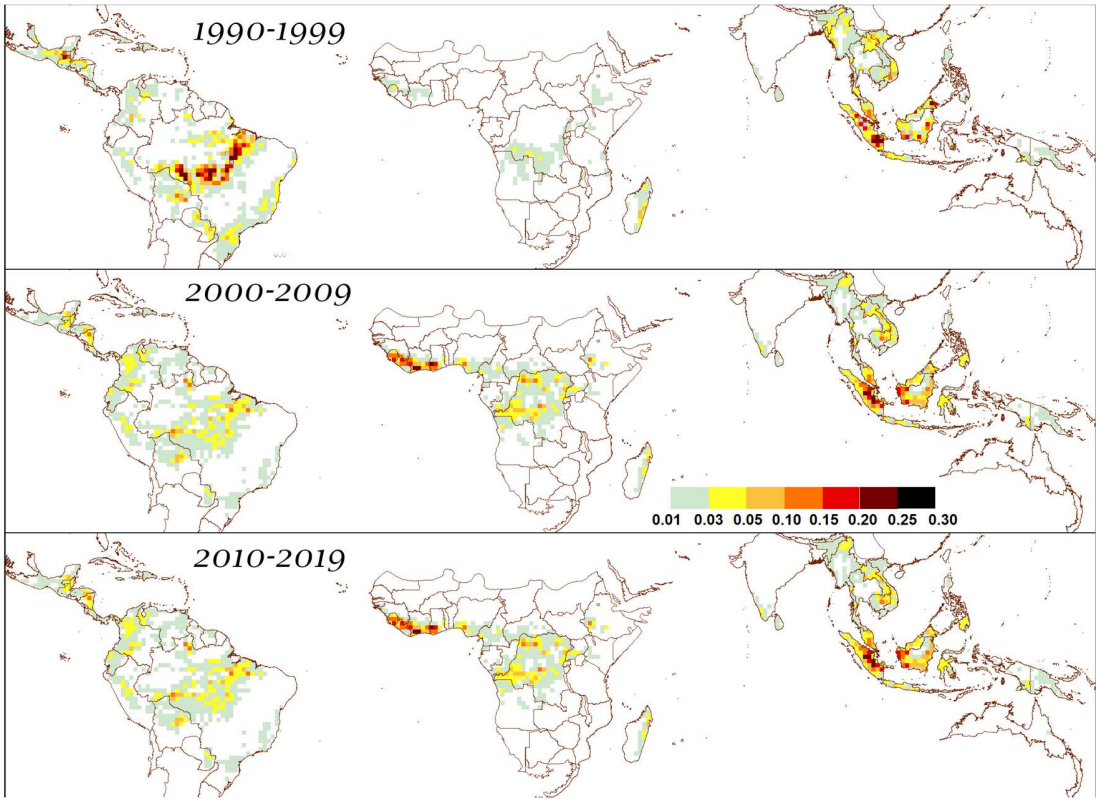

938 (A)

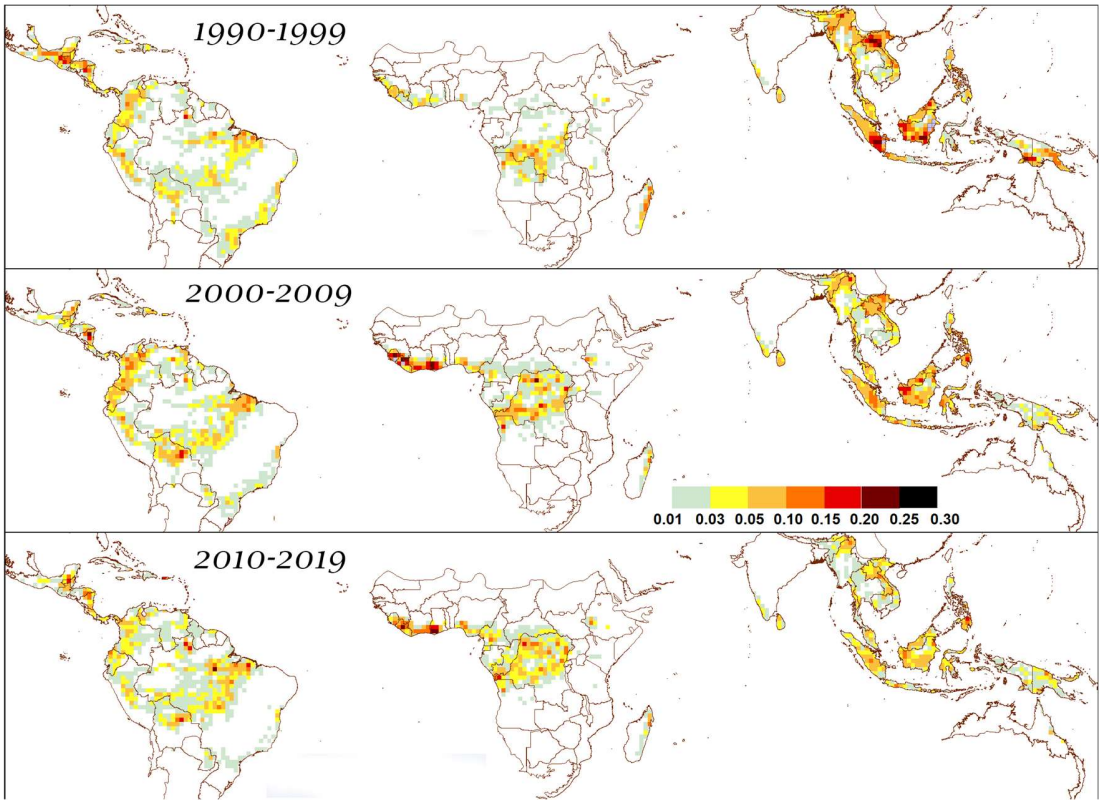

939 (B)

Table 1 Areas (in million ha) of (a) undisturbed tropical moist forests (TMF) and (b) Undisturbed and degraded TMF for years 1990, 1995, 2000, 2005, 2010, 2015 and 2020 (on first January) by sub-region and continent, and relative decline (in %) over intervals of 30 years (1990-2020), and 10 years (1990-2000, 2000-20100, 2010-2020). The values appearing in grey color indicate values derived from an average percentage of invalid pixel observations over the baseline TMF domain higher than 40%.

(a)

	Area of Undisturbed TMF on 1st January (Mha)							Decline (% of the forest)			
Sub-region	**1990**	**1995**	**2000**	**2005**	**2010**	**2015**	**2020**	**[1990-2020[**	**[1990-2000[**	**[2000-2010[**	**[2010-2020[**
West-Africa	34.6	34.1	32.8	27.4	23.9	20.6	15.6	55.0	5.0	27.1	35.0
Central-Africa	223.1	221.5	216.1	207.2	201.1	193.7	184.7	17.2	3.1	6.9	8.2
South-East Africa	15.7	15.0	12.5	10.1	8.9	7.6	6.4	59.2	20.7	28.6	27.9
Central-America	34.5	32.3	27.4	24.1	21.7	19.6	16.2	53.0	20.8	20.6	25.3
South-America	670.6	655.4	628.8	600.9	583.2	568.9	548.2	18.2	6.2	7.3	6.0
Continental SE Asia	73.3	67.2	57.7	50.2	44.4	39.9	34.2	53.3	21.2	23.2	22.9
Insular SE Asia	237.9	229.5	207.8	192.9	180.8	170.5	159.1	33.1	12.6	13.0	12.0
Continent	**1990**	**1995**	**2000**	**2005**	**2010**	**2015**	**2020**	**[1990-2020[**	**[1990-2000[**	**[2000-2010[**	**[2010-2020[**
Africa	273.4	270.6	261.4	244.7	234.0	221.9	206.7	24.4	4.4	10.5	11.7
Latin-America	705.1	687.7	656.1	625.0	604.9	588.5	564.4	19.9	6.9	7.8	6.7
Asia-Oceania	311.1	296.7	265.6	243.2	225.2	210.4	193.3	37.9	14.6	15.2	14.2
Total	1267.1	**1232.4**	**1160.6**	**1090.4**	**1041.5**	**998.2**	**964.4**	**23.9**	**8.4**	**10.3**	**7.4**

(b)

	Area of TMF (undisturbed and degraded) at the end of the year (Mha)							Decline (% of the forest)			
Sub-region	**1990**	**1995**	**2000**	**2005**	**2010**	**2015**	**2020**	**[1990-2020[**	**[1990-2000[**	**[2000-2010[**	**[2010-2020[**
West-Africa	34.6	34.3	33.3	29.8	27.4	25.1	22.1	36.0	3.6	17.8	19.3
Central-Africa	223.1	222.3	218.6	212.7	208.9	204.4	199.9	10.4	2.0	4.4	4.3
South-East Africa	15.7	15.2	12.9	11.0	10.1	9.2	8.5	45.9	17.8	21.8	15.9
Central-America	34.5	32.8	29.0	26.8	25.3	24.0	22.1	35.9	16.0	12.8	12.5
South-America	670.6	657.7	635.5	613.7	601.0	592.4	581.6	13.3	5.2	5.4	3.2
Continental SE Asia	73.3	69.1	61.3	55.7	52.0	49.2	46.4	36.6	16.3	15.2	10.6
Insular SE Asia	237.9	232.6	218.4	208.9	201.2	194.9	190.2	20.0	8.2	7.9	5.5
Continent	**1990**	**1995**	**2000**	**2005**	**2010**	**2015**	**2020**	**[1990-2020[**	**[1990-2000[**	**[2000-2010[**	**[2010-2020[**
Africa	273.4	271.7	264.8	253.5	246.4	238.7	227.7	16.7	3.1	7.0	7.6
Latin-America	705.1	690.5	664.5	640.5	626.3	616.4	599.2	15.0	5.8	5.7	4.3
Asia-Oceania	311.1	301.7	279.7	264.5	253.2	244.1	232.8	25.2	10.1	9.5	8.1
Total	1267.1	**1241.4**	**1186.5**	**1136.0**	**1103.4**	**1076.6**	**1059.6**	**16.4**	**6.4**	**7.0**	**4.0**

Table 2. Average annual losses of undisturbed tropical moist forest areas (in million ha) between 1990 and 2020 over intervals of 5 year, 30 year (1990-2020), 20 year (2000-2020), and 10 years (1990-2000,2000-2010, 2010-2020) by sub-region and continent: (a) annual losses due to deforestation and degradation, (b) annual losses due to deforestation, (c) annual losses due to degradation, (d) annual losses due to direct deforestation, (e) annual degradation before deforestation, (f) annual losses due to deforestation followed by regrowth and (g) average percentage of invalid observations over the baseline TMF domain. The values appearing in grey color indicate values derived from an average percentage of invalid observations higher than 40%.

a) total annual loss due to deforestation and degradation

	Annual loss of Undisturbed TMF areas (Mha)									
Sub-region	**[1990-1995[**	**[1995-2000[**	**[2000-2005[**	**[2005-2010[**	**[2010-2015[**	**[2015-2020[**	**[1990-2020[**	**[1990-2000[**	**[2000-2010[**	**[2010-2020[**
West-Africa	0.10	0.24	1.08	0.70	0.67	1.01	0.6	0.2	0.9	0.8
Central-Africa	0.33	1.07	1.79	1.22	1.49	1.79	1.3	0.7	1.5	1.5
South-East Africa	0.13	0.52	0.47	0.24	0.26	0.24	0.3	0.3	0.4	0.3
Central-America	0.45	0.99	0.66	0.47	0.43	0.67	0.6	0.7	0.6	0.6
South-America	3.03	5.33	5.56	3.56	2.85	4.14	4.1	4.2	4.6	4.1
Continental SE Asia	1.21	1.90	1.50	1.17	0.89	1.14	1.3	1.6	1.3	1.2
Insular SE Asia	1.68	4.32	2.98	2.43	2.07	2.28	2.6	3.0	2.7	2.5
Continent	**[1990-1995[**	**[1995-2000[**	**[2000-2005[**	**[2005-2010[**	**[2010-2015[**	**[2015-2020[**	**[1990-2020[**	**[1990-2000[**	**[2000-2010[**	**[2010-2020[**
Africa	0.56	1.82	3.34	2.15	2.42	3.04	2.2	1.2	2.7	2.6
Latin-America	3.48	6.32	6.22	4.03	3.27	4.81	4.7	4.9	5.1	4.8
Asia-Oceania	2.89	6.22	4.48	3.60	2.96	3.42	3.9	4.6	4.0	3.7
Total	6.93	**14.37**	**14.04**	**9.78**	**8.66**	**11.27**	**10.8**	**10.6**	**11.9**	**11.1**

b) annual loss due to deforestation (with or without prior degradation)

	Total deforestation on an annual basis by period (Mha)									
Sub-region	**[1990-1995[**	**[1995-2000[**	**[2000-2005[**	**[2005-2010[**	**[2010-2015[**	**[2015-2020[**	**[1990-2020[**	**[1990-2000[**	**[2000-2010[**	**[2010-2020[**
West-Africa	0.06	0.19	0.71	0.48	0.45	0.60	0.4	0.1	0.6	0.5
Central-Africa	0.17	0.74	1.18	0.76	0.90	0.91	0.8	0.5	1.0	0.9
South-East Africa	0.10	0.45	0.38	0.18	0.18	0.14	0.2	0.3	0.3	0.2
Central-America	0.34	0.76	0.45	0.29	0.26	0.37	0.4	0.6	0.4	0.3
South-America	2.57	4.44	4.35	2.54	1.73	2.16	3.0	3.5	3.4	1.9
Continental SE Asia	0.84	1.55	1.13	0.74	0.56	0.54	0.9	1.2	0.9	0.6
Insular SE Asia	1.05	2.83	1.91	1.53	1.27	0.94	1.6	1.9	1.7	1.1
Continent	**[1990-1995[**	**[1995-2000[**	**[2000-2005[**	**[2005-2010[**	**[2010-2015[**	**[2015-2020[**	**[1990-2020[**	**[1990-2000[**	**[2000-2010[**	**[2010-2020[**
Africa	0.33	1.38	2.26	1.42	1.54	1.65	1.43	0.86	1.84	1.59
Latin-America	2.91	5.21	4.80	2.83	1.99	2.53	3.38	4.06	3.82	2.26
Asia-Oceania	1.89	4.38	3.04	2.27	1.83	1.48	2.48	3.14	2.65	1.65
Total	5.14	**10.97**	**10.10**	**6.52**	**5.35**	**5.66**	**7.29**	**8.06**	**8.31**	**5.51**

c) annual loss due to degradation (followed or not by deforestation)

	Total degradation on an annual basis by period (Mha)									
Sub-region	**[1990-1995[**	**[1995-2000[**	**[2000-2005[**	**[2005-2010[**	**[2010-2015[**	**[2015-2020[**	**[1990-2020[**	**[1990-2000[**	**[2000-2010[**	**[2010-2020[**
West-Africa	0.08	0.16	0.87	0.50	0.35	0.61	0.4	0.1	0.7	0.5
Central-Africa	0.28	0.83	1.40	0.91	0.92	1.24	0.9	0.6	1.2	1.1
South-East Africa	0.09	0.27	0.28	0.14	0.13	0.13	0.2	0.2	0.2	0.1
Central-America	0.29	0.64	0.49	0.34	0.27	0.45	0.4	0.5	0.4	0.4
South-America	1.25	2.29	2.61	1.83	1.59	2.54	2.0	1.8	2.2	2.1
Continental SE Asia	0.88	1.23	1.03	0.81	0.49	0.78	0.9	1.1	0.9	0.6
Insular SE Asia	1.16	2.80	1.98	1.39	1.03	1.65	1.7	2.0	1.7	1.3
Continent	**[1990-1995[**	**[1995-2000[**	**[2000-2005[**	**[2005-2010[**	**[2010-2015[**	**[2015-2020[**	**[1990-2020[**	**[1990-2000[**	**[2000-2010[**	**[2010-2020[**
Africa	0.45	1.26	2.56	1.55	1.40	1.98	1.53	0.86	2.05	1.69
Latin-America	1.54	2.93	3.10	2.16	1.85	2.99	2.43	2.24	2.63	2.42
Asia-Oceania	2.04	4.03	3.00	2.21	1.51	2.43	2.54	3.04	2.61	1.97
Total	4.03	**8.23**	**8.66**	**5.92**	**4.77**	**7.40**	**6.50**	**6.13**	**7.29**	**6.09**

d) annual loss due to direct deforestation (without prior degradation)

	Annual direct deforestation by period (Mha)									
Sub-region	**[1990-1995[**	**[1995-2000[**	**[2000-2005[**	**[2005-2010[**	**[2010-2015[**	**[2015-2020[**	**[1990-2020[**	**[1990-2000[**	**[2000-2010[**	**[2010-2020[**
West-Africa	0.02	0.08	0.21	0.19	0.32	0.40	0.2	0.0	0.2	0.4
Central-Africa	0.05	0.24	0.38	0.31	0.57	0.56	0.4	0.1	0.3	0.6
South-East Africa	0.05	0.24	0.19	0.10	0.13	0.10	0.1	0.1	0.1	0.1
Central-America	0.16	0.34	0.17	0.13	0.16	0.22	0.2	0.2	0.2	0.2
South-America	1.78	3.05	2.95	1.73	1.26	1.61	2.1	2.4	2.3	1.4
Continental SE Asia	0.33	0.66	0.48	0.36	0.41	0.36	0.4	0.5	0.4	0.4
Insular SE Asia	0.52	1.53	1.00	1.03	1.04	0.62	1.0	1.0	1.0	0.8
Continent	**[1990-1995[**	**[1995-2000[**	**[2000-2005[**	**[2005-2010[**	**[2010-2015[**	**[2015-2020[**	**[1990-2020[**	**[1990-2000[**	**[2000-2010[**	**[2010-2020[**
Africa	0.11	0.56	0.78	0.60	1.02	1.06	0.69	0.34	0.69	1.04
Latin-America	1.94	3.39	3.12	1.86	1.42	1.82	2.26	2.66	2.49	1.62
Asia-Oceania	0.85	2.19	1.48	1.39	1.45	0.99	1.39	1.52	1.44	1.22
Total	2.90	**6.14**	**5.38**	**3.86**	**3.89**	**3.87**	**4.34**	**4.52**	**4.62**	**3.88**

e) annual degradation before deforestation

	Annual degradation before deforestation by period (Mha)									
Sub-region	**[1990-1995[**	**[1995-2000[**	**[2000-2005[**	**[2005-2010[**	**[2010-2015[**	**[2015-2020[**	**[1990-2020[**	**[1990-2000[**	**[2000-2010[**	**[2010-2020[**
West-Africa	0.04	0.11	0.50	0.28	0.14	0.20	0.2	0.1	0.4	0.2
Central-Africa	0.12	0.50	0.79	0.45	0.33	0.35	0.4	0.3	0.6	0.3
South-East Africa	0.06	0.21	0.19	0.08	0.05	0.04	0.1	0.1	0.1	0.0
Central-America	0.18	0.42	0.28	0.16	0.10	0.16	0.2	0.3	0.2	0.1
South-America	0.79	1.40	1.40	0.81	0.47	0.55	0.9	1.1	1.1	0.5
Continental SE Asia	0.51	0.89	0.65	0.38	0.15	0.18	0.5	0.7	0.5	0.2
Insular SE Asia	0.53	1.31	0.91	0.50	0.23	0.31	0.6	0.9	0.7	0.3
Continent	**[1990-1995[**	**[1995-2000[**	**[2000-2005[**	**[2005-2010[**	**[2010-2015[**	**[2015-2020[**	**[1990-2020[**	**[1990-2000[**	**[2000-2010[**	**[2010-2020[**
Africa	0.22	0.82	1.48	0.82	0.52	0.59	0.74	0.52	1.15	0.55
Latin-America	0.98	1.82	1.68	0.97	0.57	0.71	1.12	1.40	1.33	0.64
Asia-Oceania	1.05	2.19	1.56	0.88	0.38	0.49	1.09	1.62	1.22	0.44
Total	2.24	**4.83**	**4.72**	**2.66**	**1.47**	**1.79**	**2.95**	**3.54**	**3.69**	**1.63**

f) annual deforestation followed by a regrowth

	Total deforestation followed by regrowth on an annual basis by period (Mha)									
Sub-region	**[1990-1995[**	**[1995-2000[**	**[2000-2005[**	**[2005-2010[**	**[2010-2015[**	**[2015-2020[**	**[1990-2020[**	**[1990-2000[**	**[2000-2010[**	**[2010-2020[**
West-Africa	0.00	0.00	0.01	0.04	0.06	0.03	0.0	0.0	0.0	0.0
Central-Africa	0.02	0.04	0.07	0.10	0.13	0.06	0.1	0.0	0.1	0.1
South-East Africa	0.00	0.01	0.02	0.03	0.03	0.01	0.0	0.0	0.0	0.0
Central-America	0.05	0.09	0.07	0.07	0.05	0.02	0.1	0.1	0.1	0.0
South-America	0.21	0.40	0.50	0.49	0.37	0.20	0.4	0.3	0.5	0.3
Continental SE Asia	0.10	0.20	0.24	0.23	0.14	0.06	0.2	0.2	0.2	0.1
Insular SE Asia	0.11	0.33	0.44	0.42	0.30	0.15	0.3	0.2	0.4	0.2
Continent	**[1990-1995[**	**[1995-2000[**	**[2000-2005[**	**[2005-2010[**	**[2010-2015[**	**[2015-2020[**	**[1990-2020[**	**[1990-2000[**	**[2000-2010[**	**[2010-2020[**
Africa	0.02	0.06	0.10	0.17	0.21	0.10	0.11	0.04	0.13	0.15
Latin-America	0.26	0.48	0.58	0.56	0.43	0.22	0.42	0.37	0.57	0.32
Asia-Oceania	0.21	0.53	0.68	0.65	0.44	0.21	0.45	0.37	0.66	0.32
Total	0.50	**1.06**	**1.36**	**1.37**	**1.08**	**0.53**	**0.98**	**0.78**	**1.37**	**0.80**

g) average percentage of invalid observations over the TMF domain per period and per year

	Average % of Invalid observations (over the total forest domain, per period)						
Sub-region	**[1982-1990[**	**[1990-1995[**	**[1995-2000[**	**[2000-2005[**	**[2005-2010[**	**[2010-2015[**	**[2015-2020[**
West-Africa	98.1	87.1	82.5	40.0	2.8	0.4	0.0
Central-Africa	99.4	94.7	80.8	37.2	6.7	2.9	0.4
South-East Africa	97.9	80.8	20.7	3.9	1.3	0.8	0.1
Central-America	50.1	12.4	4.3	1.2	0.4	0.1	0.0
South-America	30.5	1.2	0.6	0.2	0.0	0.0	0.0
Continental SE Asia	54.5	14.6	1.3	0.4	0.0	0.0	0.0
Insular SE Asia	34.3	16.3	4.2	0.8	0.1	0.1	0.0
Continent	**[1982-1990[**	**[1990-1995[**	**[1995-2000[**	**[2000-2005[**	**[2005-2010[**	**[2010-2015[**	**[2015-2020[**
Africa	99.1	92.9	77.6	35.7	5.9	2.4	0.3
Latin-America	31.3	1.6	0.8	0.2	0.1	0.0	0.0
Asia-Oceania	29.5	12.0	3.7	1.3	0.3	0.2	0.0
Total	**21.2**	31.9	**23.1**	**10.1**	**2.3**	**0.8**	**0.1**

	Average % of Invalid observations (over the total forest domain, per year)							
Sub-region	**1982**	**1990**	**1995**	**2000**	**2005**	**2010**	**2015**	**2019**
West-Africa	100.0	90.8	84.3	71.8	5.9	0.7	0.2	0.0
Central-Africa	100.0	97.7	87.6	67.8	10.2	3.7	1.9	0.0
South-East Africa	100.0	92.1	41.5	8.4	1.5	1.0	0.5	0.0
Central-America	69.4	17.0	5.8	1.8	0.7	0.2	0.0	0.0
South-America	55.6	1.7	0.8	0.3	0.1	0.0	0.0	0.0
Continental SE Asia	55.2	49.1	2.0	1.0	0.0	0.0	0.0	0.0
Insular SE Asia	34.6	31.2	6.5	1.9	0.2	0.1	0.0	0.0
Continent	**1982**	**1990**	**1995**	**2000**	**2005**	**2010**	**2015**	**2019**
Africa	100.0	93.5	71.2	49.3	5.9	1.8	0.9	0.0
Latin-America	62.5	9.4	3.3	1.0	0.4	0.1	0.0	0.0
Asia-Oceania	44.9	40.2	4.3	1.4	0.1	0.1	0.0	0.0
Total	**69.1**	**47.7**	**26.2**	**17.3**	**2.1**	**0.7**	**0.3**	**0.0**

Table 3. Total areas and proportions of tropical moist forest disturbances (deforestation without regrowth, regrowth after deforestation, forest degradation) and reforestation areas (initially other land cover) over the period 1990-2020 for each sub-region and continent (areas in million ha and proportions in percentage).

	Disturbed areas (Mha)				% of Tot disturbances			% of Undisturbed Forest in 1990				
Sub-region	**Deforestation**	**Regrowth**	**Degradation**	**Total**	**Deforestation**	**Regrowth**	**Degradation**	**Deforestation**	**Regrowth**	**Degradation**	**Total**	**Reforestation (from other LC)**
West-Africa	11.8	0.7	6.5	19.0	61.9	3.7	34.5	34.0	2.0	18.9	55.0	0.4
Central-Africa	21.2	2.1	15.1	38.4	55.2	5.4	39.4	9.5	0.9	6.8	17.2	1.1
South-East Africa	6.7	0.5	2.1	9.3	71.9	5.7	22.4	42.5	3.4	13.3	59.2	0.2
Central-America	10.6	1.8	5.9	18.3	58.0	9.7	32.3	30.7	5.1	17.1	53.0	0.7
South-America	78.1	10.9	33.4	122.4	63.8	8.9	27.3	11.6	1.6	5.0	18.2	4.0
Continental SE Asia	22.0	4.9	12.2	39.1	56.2	12.4	31.4	30.0	6.6	16.7	53.3	2.0
Insular SE Asia	38.9	8.7	31.1	78.8	49.4	11.1	39.5	16.4	3.7	13.1	33.1	1.6
Continent	**Deforestation**	**Regrowth**	**Degradation**	**Total**	**Deforestation**	**Regrowth**	**Degradation**	**Deforestation**	**Regrowth**	**Degradation**	**Total**	**Reforestation (from other LC)**
Africa	39.6	3.3	23.8	66.7	59.4	4.9	35.6	14.5	1.2	8.7	24.4	1.6
Latin-America	88.7	12.6	39.3	140.7	63.1	9.0	27.9	12.6	1.8	5.6	19.9	4.7
Asia-Oceania	60.9	13.6	43.4	117.8	51.7	11.5	36.8	19.6	4.4	13.9	37.9	3.6
Total	189.2	29.5	106.5	325.2	58.2	9.1	32.7	14.9	2.3	8.4	25.7	10.0

1000 **Table 4.** Comparison of estimates of annual deforested areas (in million ha / year) from previous
1001 studies and our study, over the tropical belt, over the three continents and Brazil.

Source		Hansen et al. 2013		Tyukavina et al. 2015	Keenan et al. 2015	PRODES-INPE	This Study		
Forest extent		Whole TMF (undisturbed and degraded)	Primary forest from INPE	Natural forests *	All tropical forests (evergreen & deciduous)	Primary forest	Tropical moist forest	TMF excluding the tree plantations	Primary forest from INPE
Pan-tropical region	2001-2010	4.67			7.24		7.72		
	2001-2012	4.80		6.5 ± 0.7			7.19	6.44	
	2001-2015	5.07			6.66		6.95		
	2010-2019	6.87					5.51		
	2001-2019	5.79					6.66		
Africa	2001-2012	0.73		1.21 ± 0.4			1.60	1.57	
	2001-2019	1.28					1.64		
Latin America	2001-2012	2.19		3.7 ± 0.5			3.25	3.19	
	2001-2019	2.41					2.93		
Asia - Oceania	2001-2012	1.89		1.6 ± 0.4			2.34	1.67	
	2001-2019	2.10					2.09		
Brazil	2001-2010	1.61	1.35			1.65	2.55		1.57
	2001-2012	1.54	1.26	2.1 ± 0.3		1.47	2.32	2.27	1.42
	2010-2019	1.64	1.34			0.67	1.63		1.04
	2001-2019	1.64	1.35			1.19	2.10		1.31

1002
1003